frontiers in MICROBIOLOGY

REVIEW ARTICLE
published: 13 January 2012
doi: 10.3389/fmicb.2011.00279

Wild-type measles virus is intrinsically dual-tropic

Makoto Takeda[1]*, Maino Tahara[1], Noriyo Nagata[2] and Fumio Seki[1]

[1] Department of Virology 3, National Institute of Infectious Diseases, Tokyo, Japan
[2] Department of Pathology, National Institute of Infectious Diseases, Tokyo, Japan

Edited by:
Yasuko Yokota, National Institute of Infectious Diseases, Japan

Reviewed by:
Masato Tsurudome, Mie University Graduate School of Medicine, Japan
Bert Rima, Queen's University Belfast, UK

***Correspondence:**
Makoto Takeda, Department of Virology 3, National Institute of Infectious Diseases, Gakuen 4-7-1, Musashimurayama, Tokyo 208-0011, Japan.
e-mail: mtakeda@nih.go.jp

Measles is a highly contagious disease that causes temporary and severe immunosuppression in patients. Signaling lymphocyte activation molecule (SLAM) expressed on cells of the immune system functions as a receptor for measles virus (MV). In addition to SLAM, vaccine strains of MV also use a ubiquitously expressed complement regulatory protein, CD46, as a receptor, whereas wild-type (wt) MV strains do not use this receptor. However, recent studies have indicated that SLAM is not the sole receptor for wt MV strains. These strains have an intrinsic ability to enter both immune and epithelial cells using distinct receptor binding sites in their hemagglutinin (H) protein. Recently, a clear answer was obtained through the identification of an epithelial MV receptor, nectin4, expressed at adherens junctions, thereby greatly improving our knowledge of MV receptors. It is now clear that MV specifically targets two cell types, immune cells and epithelial cells, using SLAM and nectin4, respectively. MV loses the ability to use either SLAM or nectin4 when it possesses specific mutations in the H protein. However, nectin4-blind MV still infects SLAM-positive immune cells efficiently (SLAM-tropic), and conversely, SLAM-blind MV infects nectin4-positive epithelial cells efficiently (nectin4-tropic). In this regard, MV is intrinsically dual-tropic to immune cells and epithelial cells. Although many aspects and molecular mechanisms underlying immunosuppressive effects and a highly contagious nature of MV still remain to be elucidated, analyses of physiological functions of these two receptors would provide deep insights into MV pathogenesis.

Keywords: measles virus, dual-tropic, SLAM, nectin4, receptor

MEASLES VIRUS

Measles is a highly contagious acute viral disease characterized by high fever, malaise, coryza, conjunctivitis, cough, and a maculopapular rash (Griffin, 2007). Patients with measles develop a severe and temporary immunosuppression, which is often accompanied by secondary bacterial infections (Griffin, 2007). Despite the availability of highly effective vaccines, measles-related deaths were estimated to be 164,000 worldwide in 2008 (WHO, 2009). The causative agent is measles virus (MV), which belongs to the genus *Morbillivirus* in the family *Paramyxoviridae*. The virus particle is enveloped and contains a non-segmented negative-strand RNA genome encoding six tandem linked genes, N, P/V/C, M, F, H, and L. The genome is encapsidated by the nucleocapsid (N) protein and associated with viral RNA-dependent RNA polymerases, forming a helical ribonucleoprotein complex (RNP). On the envelope, the viral particle possesses two types of viral glycoprotein spikes, the hemagglutinin (H) and fusion (F) proteins (Griffin, 2007). The H protein is responsible for binding to cellular receptors on the target host cells, and plays a key role in the determination of host cell specificity (tropism) of MV (Yanagi et al., 2009). Binding of the H protein to a receptor triggers F protein-mediated membrane fusion between the virus envelope and the host cell plasma membrane, releasing the RNP into the cytoplasm. In cells infected with MV, the H and F proteins are expressed on the cell surface and cause cell-to-cell fusion, producing syncytia.

DISCOVERIES OF CELLULAR RECEPTORS FOR MV

Basically, MV specifically infects cells expressing its receptors. Therefore, the distribution pattern of its receptors is a key determinant of which cells become infected with MV (Yanagi et al., 2009). The initial discovery of an MV receptor came in 1993 (Dorig et al., 1993; Naniche et al., 1993). Two independent studies indicated that the receptor molecule for MV is the human membrane cofactor protein (MCP/CD46), a central component of the complement system, which is expressed ubiquitously on all organs and tissues throughout the human body (Dorig et al., 1993; Naniche et al., 1993). These findings were highly welcomed from the viewpoint that MV causes a systemic infection. Meanwhile, Kobune et al. (1990) reported the isolation of lymphotropic MV strains, and subsequent studies indicated that these lymphotropic MV strains do not use MCP/CD46 as a receptor (Yanagi et al., 2009). Importantly, Kobune's isolates exhibited a high virulence in experimentally infected monkeys, whereas MCP/CD46-using classical MV isolates caused no or mild disease in monkeys (Kobune et al., 1990, 1996; Takeda et al., 1998). Hence, new two questions have arisen for MV researchers. What is the receptor for these lymphotropic strains? Which strains are the real wild-type (wt) MV strains? In 2000, using Kobune's isolates, another receptor was identified (Tatsuo et al., 2000). This receptor is signaling lymphocyte activation molecule, also known as CD150 (SLAM/CD150), which is expressed on cells of the immune system (Tatsuo et al., 2000). Subsequent studies clarified

that SLAM/CD150 is a receptor for wt MV strains circulating in patients, and that MCP/CD46 does not act as a receptor for wt MV strains (Yanagi et al., 2009). MCP/CD46 acts as a receptor only for vaccine and some laboratory MV strains (Yanagi et al., 2009). Currently, it is clear that these MV strains have acquired the ability to use MCP/CD46 as an alternative receptor to grow in laboratory cell lines lacking SLAM/CD150 expression (Yanagi et al., 2009).

Hence, it has become generally accepted that wt MV is a lymphotropic virus that specifically targets immune cells, similar to the case of human immunodeficiency virus (HIV) and human T cell lymphotropic virus type 1 (HTLV1). In 2000, a recombinant MV, IC323, was generated based on Kobune's first isolate (Takeda et al., 2000), and has greatly contributed to our understanding of the molecular bases for the pathogenesis of wt MV strains (Takeuchi et al., 2005; de Swart et al., 2007; Devaux et al., 2008, 2011; Leonard et al., 2008; Nakatsu et al., 2008; de Vries et al., 2010; Ludlow et al., 2010; Mühlebach et al., 2011; Noyce et al., 2011). At that time, only SLAM/CD150-positive cells were found to be susceptible to wt MV infections. However, it remained difficult to make a final conclusion that SLAM/CD150 is the sole receptor for wt MV, because histopathological examinations of measles patients and monkeys infected with MV have revealed considerable levels of MV protein expression in the epithelia of various organs, and histopathological changes are also evident in these epithelia (Nii et al., 1964; Lightwood and Nolan, 1970; Olding-Stenkvist and Bjorvatn, 1976; Moench et al., 1988; Craighead, 2000; **Figure 1**). In 2003, primary cultures of human small airway epithelial cells (SAECs) were shown to be susceptible to wt MV infection (Takeuchi et al., 2003). Upon MV infection, large syncytia developed in SAECs via a SLAM-independent mechanism (Takeuchi et al., 2003). After searching many cell lines, several epithelial cell lines with high susceptibility to MV infection were identified (Takeda et al., 2007; Tahara et al., 2008). Tahara et al. (2008) and Leonard et al. (2008) clearly demonstrated that wt MV infects epithelial cell lines that form tight junctions (TJs) using an unidentified receptor (Leonard et al., 2008; Tahara et al., 2008). Using these cells and recombinant IC323 expressing green fluorescent protein (IC323-EGFP; Takeda et al., 2000; Hashimoto et al., 2002), a final answer was obtained for the receptor on epithelial cells. Two groups independently demonstrated that nectin4, which is expressed at adherens junctions (AJs), acts as a receptor for MV (Mühlebach et al., 2011; Noyce et al., 2011). Interestingly, MV loses the ability to use either SLAM/CD150 or nectin4 when it possesses specific mutations in the H protein (Leonard et al., 2008; Tahara et al., 2008; **Figure 2**). Nectin4-blind MV still infects SLAM/CD150-positive immune cells efficiently (SLAM/CD150-tropic), and conversely, SLAM/CD150-blind MV infects nectin4-positive epithelial cells efficiently (nectin4-tropic; Leonard et al., 2008; Tahara et al., 2008; **Figure 2**). In this regard, MV is intrinsically dual-tropic to immune cells and epithelial cells (**Figure 2**).

There is now no doubt that SLAM/CD150 and nectin4 are the major receptors for MV. However, other molecules may further support MV infection *in vivo*, being involved in the development of measles and its neurological sequela. For example, the mechanism that the C-type lectin DC-specific intercellular adhesion molecule 3-grabbing non-integrin (DC-SIGN) acts as an attachment receptor for MV, thereby promoting MV infection of DCs, may be ideal to understand the extraordinarily high transmissibility of measles (de Witte et al., 2006, 2008). It is well known that MV causes subacute sclerosing panencephalitis (SSPE), a persistent infection of the central nervous system (CNS) with MV. This occurs with a mean latency period of 7–10 years after suffering from acute measles at a frequency of 1/5,000–1/100,000 reported cases of acute measles (Takasu et al., 2003; Bellini et al., 2005). The mechanisms underlying the spread of MV in the CNS remain to be elucidated. Although nectin4 is a possible candidate for an MV receptor in the CNS, no (or undetectable) nectin4 expression was observed in the CNS in humans (Reymond et al., 2001; Brancati et al., 2010), and some MV strains derived from SSPE patients are likely to use nectin4 inefficiently (Seki et al., 2011). Data reported by Makhortova et al. (2007) suggest that neurokinin-1, a substance P receptor, supports trans-synaptic transmission of MV by acting as a receptor for the F protein.

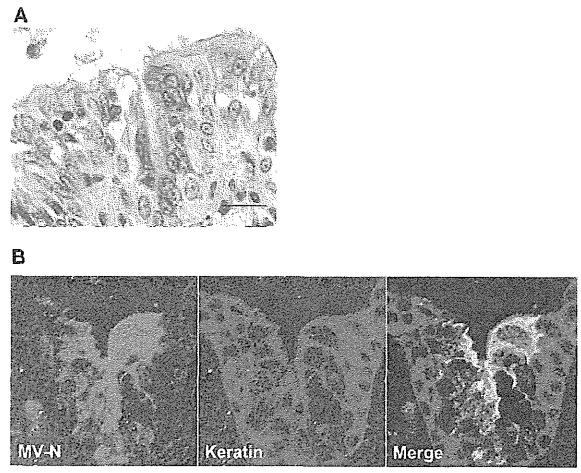

FIGURE 1 | Measles virus antigen and histopathological changes in bronchiolar epithelial cells. At 11 days post-infection, a cynomolgus monkey experimentally infected with wt MV IC323 strain was subjected to the histopathological examination. **(A)** Hematoxylin and eosin staining. Multinucleated cell were seen in the epithelial layer of the bronchiole with inflammatory infiltration of eosinophils and lymphocytes. The multinucleated cells contain eosinophilic intranuclear inclusions. Scale bar indicates 20μm. **(B)** Immunohistochemical double staining for the N protein of MV (left, green) and keratin (center, red). Multinucleated epithelial giant cells showing positive staining for the N protein are present in the bronchiole (right, yellow in merged images). Accumulation of N proteins is detected on the apical surface of ciliated epithelial cells.

SLAM/CD150

Measles virus infection causes immunosuppression in patients and is often accompanied by secondary bacterial infections. Typically, MV-induced immunosuppression is characterized by a marked lymphopenia, and an early T_H1 response followed by predominant and prolonged T_H2 response in patients, with suppression of mitogen-induced lymphocyte proliferation *ex vivo* (Griffin and

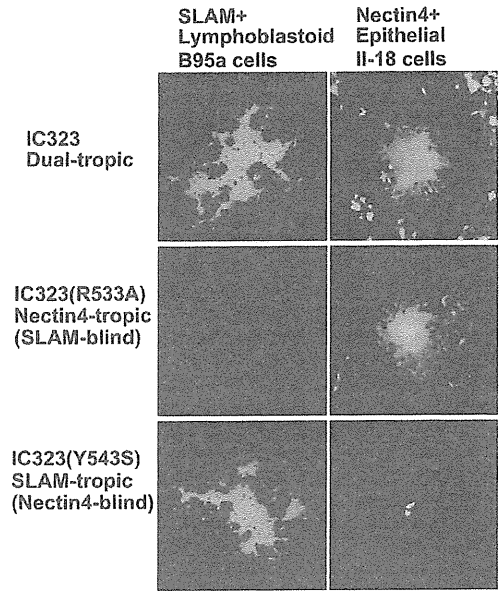

FIGURE 2 | Dual-tropic nature of wt MV. Wt MV (IC323) infects and produces syncytia in both SLAM-positive lymphoblastoid B95a and nectin4-positive epithelial II-18 cells (dual-tropic). IC323 with an R533A mutation in the H protein fails to spread in B95a cells (SLAM-blind), but replicates well in II-18 cells (nectin4-tropic). On the contrary, IC323 with a Y543S mutation in the H protein spreads in B95a cells (SLAM-tropic), but fails to spread in II-18 cells (nectin4-blind). All MVs in this figure are engineered to express EGFP.

Ward, 1993; Schneider-Schaulies and Schneider-Schaulies, 2009). Some, if not all, of these immunological observations must be attributed either directly or indirectly to the fact that MV uses SLAM/CD150 as a receptor. SLAM/CD150 is a member of the SLAM-family receptors, which belong to the immunoglobulin (Ig) superfamily (Veillette, 2010; Ma and Deenick, 2011). The SLAM-family consists of nine members (Cannons et al., 2011; Ma and Deenick, 2011). The SLAM-family receptors are type I transmembrane proteins that typically possess an extracellular region with two Ig-like domains (an amino-terminal variable (V)-like domain and a carboxy-terminal constant-2 (C2)-like domain), a transmembrane region, and a cytoplasmic region that harbors multiple tyrosine-based motifs (Detre et al., 2010; Veillette, 2010; Cannons et al., 2011; Ma and Deenick, 2011). These motifs are referred to as immunoreceptor tyrosine-based switch motifs (ITSMs; Cannons et al., 2011). The SLAM-family receptors are expressed in a broad range of immune cells and play critical roles in immunity. In general, the receptors act as self-ligands and their homophilic *trans*-interactions occur between either heterotypic or homotypic immune cells (Veillette, 2010; Ma and Deenick, 2011). SLAM/CD150 is expressed on thymocytes, subsets of B and T lymphocytes, mature dendritic cells (DCs), macrophages, and platelets, and their expression is upregulated or induced in lymphocytes and monocytes upon activation (Detre et al., 2010; Veillette, 2010; Cannons et al., 2011; Ma and Deenick, 2011).

Signaling lymphocyte activation molecule-associated protein (SAP)-family adaptors [SAP, Ewing's sarcoma-associated transcript (EAT)-2, and EAT-2-related transducer (ERT)] play important roles for the signal transductions mediated by the SLAM-family receptors (Veillette, 2010; Ma and Deenick, 2011). They are small proteins that consist of a single Src homology 2 (SH2) domain and a short carboxy-terminal region. SAP associates intracellularly with the ITSMs in the cytoplasmic region of the SLAM-family receptors via the SH2 domain (Dong and Veillette, 2010; Veillette, 2010; Ma and Deenick, 2011). SAP has the ability to bind concomitantly to the Src-family protein tyrosine kinase, Fyn, thereby coupling the SLAM-family receptors with Fyn (Dong and Veillette, 2010; Veillette, 2010; Cannons et al., 2011). Thereafter, Fyn phosphorylates tyrosine residues at the cytoplasmic region of SLAM-family receptors and other intracellular effector molecules, activating the downstream signals (Detre et al., 2010; Dong and Veillette, 2010; Cannons et al., 2011; Ma and Deenick, 2011). In another mechanism, SAP binding to the SH2 domain of SLAM-family receptors competes with the binding of other SH2 domain-containing molecules, thus modulating the SLAM-mediated signaling (Dong and Veillette, 2010; Veillette, 2010; Cannons et al., 2011). In $CD4^+$ T cells, signals via SLAM/CD150-SAP–Fyn interactions play important roles in regulating T cell receptor-mediated induction of T_H2 cytokines, such as interleukin (IL)-4 and IL-13 (Detre et al., 2010; Cannons et al., 2011; Ma and Deenick, 2011). EAT-2 also mediates the signal transduction cascades of the SLAM-family receptors via a similar but distinct mechanism to that of SAP (Cannons et al., 2011). Similar to SAP, EAT-2 also associates with the ITSMs of SLAM-family receptors through its SH2 domain, but mediates the subsequent signal cascades via its own phosphorylated tyrosine in the short carboxy-terminal region (Veillette, 2010). In general, the signals mediated by the SAP-family adaptors induce the activation and differentiation of immune cells (Veillette, 2010). However, if the SAP-family adaptors are absent, the SLAM-family receptors mediate inhibitory signals to immune cells (a switch-of-function effect; Dong and Veillette, 2010; Veillette, 2010).

Roles for SLAM/CD150 in macrophage functions, cell adhesion, and NKT cell development have also been demonstrated, although many data were obtained in mice (Dong and Veillette, 2010; Veillette, 2010; Cannons et al., 2011; Ma and Deenick, 2011). X-linked lymphoproliferative syndrome is a rare immunodeficiency disease typically caused by mutations in the SAP-encoding gene, *SH2D1A* (Veillette, 2010; Ma and Deenick, 2011). Patients with this syndrome have various functional defects and impaired differentiation of immune cells, indicating crucial roles for SAP in normal immunity (Dong and Veillette, 2010). Hypogammaglobulinemia, massive lymphoproliferative syndrome, and a fatal response to Epstein–Barr virus infection are characteristics of the disease (Veillette, 2010; Ma and Deenick, 2011). Although SLAM-family receptors have some functional redundancy, each receptor plays specific roles in a variety of immune responses (Dong and Veillette, 2010; Veillette, 2010).

NECTIN4

In general, lymphotropic viruses, such as HIV and HTLV1, can never be airborne, and are transmitted inefficiently even through

direct contact with patients. In sharp contrast, MV transmits via aerosols, and has a highly contagious nature. Therefore, this transmission style of MV cannot be easily explained by the fact that the virus uses a lymphocytic molecule, SLAM/CD150, as a receptor. The recent findings showing that MV uses nectin4, a cell adhesion molecule (CAM) expressed at the AJs of epithelia, may partly but nicely explain how and why MV transmits efficiently from a patient to other individuals. Epithelial cells are connected with one another through the formation of several specialized cell–cell junctions, such as TJs, AJs, desmosomes, and gap junctions. TJs function as a physical barrier that prevents the passage of soluble molecules through the intercellular gaps, and also blocks the lateral movement of lipids and membrane proteins across the TJ barrier, thereby acting as the border of the apical and basolateral membranes. AJs are located near the basolateral side of the TJs. They are basically formed by cadherins and nectins and intracellularly connected by actin filaments. Nectin4 is a member of the nectin family, which consists of four members (nectin1, 2, 3, and 4; Takai et al., 2008a). Nectin1 and nectin2 were originally identified as poliovirus receptor-related protein (PRR)-1 and PRR-2, respectively, and subsequently shown to support the entry of some herpes viruses (Takai et al., 2008a,b). Similar to the SLAM-family members, nectins are also type I transmembrane proteins that belong to the Ig superfamily (Takai et al., 2008a,b). In general, they possess an extracellular region with three Ig-like domains (an amino-terminal V-like domain and two C-like domains), a transmembrane region, and a cytoplasmic region with a short afadin-binding motif (Takai et al., 2008a,b). The consensus motif was reported to be E/A-X-Y-V for nectin1, 2, and 3, while nectin4 does not have this motif but still binds to afadin (Reymond et al., 2001; Takai et al., 2008a). Reymond et al. (2001) proposed a new consensus motif, K/R-X-X-Y/L-V, for all four nectins. Afadin is an actin filament (F-actin)-binding protein, and supports nectins to interact and co-operate with cadherins, other CAMs, and intracellular signaling molecules (Takai et al., 2008a).

Nectins are expressed as dimers, and interact *in trans* with other nectin dimers expressed on neighboring cells (Takai et al., 2008a,b). All nectins show homophilic interactions, while heterophilic interactions are also observed between specific nectins, such as those between nectin1/nectin3 and nectin 2/nectin3 (Takai et al., 2008a,b). Some nectin-like molecules also interact with nectins (Takai et al., 2008a,b). Nectin4 shows homophilic interactions as well as heterophilic interactions with nectin1 (Reymond et al., 2001; Takai et al., 2008a). The Ig V-like domain is used for the *trans*-interaction (Reymond et al., 2001; Fabre et al., 2002). Nectins play key roles in the initiation of AJ formation, and regulate various physiological functions of epithelial cells, such as contact inhibition of cell movement and proliferation, survival, differentiation, and cell polarization (Takai et al., 2008a,b).

Although nectin1 and nectin2 are expressed in a broad range of tissues, the expression of nectin3 and nectin4 is more specific (Reymond et al., 2001). Reymond et al. (2001) and Brancati et al. (2010) showed that human nectin4 is expressed mainly in the placenta and to lesser extents in the trachea, prostate, lung, and stomach. In addition, Brancati et al. (2010) demonstrated nectin4 expression in human keratinocytes, suprabasal nucleated layers of the epidermis, and non-keratinized structures of hair. Some levels of expression in epithelial cells of the tonsil, oral mucosa, esophagus, and nasopharynx have also been reported (www.proteinatlas.org). Although, in many cases, nectin4 is expressed in low or undetectable levels in normal human tissues, many cancer cells are highly positive for nectin4. Thus, it has been proposed that nectin4 is a new tumor-associated marker (Fabre-Lafay et al., 2007; Takano et al., 2009; Derycke et al., 2010). These observations may provide a rationale for the use of MV as an oncolytic agent (Mühlebach et al., 2011). In humans, mutations in the *PVRL4* gene encoding nectin4 cause ectodermal-dysplasia-syndactyly syndrome (EDSS), in which patients have affected skin and skin appendages, such as hair, teeth, and nails (Brancati et al., 2010; Jelani et al., 2011).

RELEVANCE OF SLAM/CD150 AND NECTIN4 TO MV PATHOGENESIS

The pathology of measles can now be drawn with these two receptors (**Figure 3**). Although nectin4-expressing epithelial cells can be the initial targets of MV, no or very limited infection of epithelia was observed in monkeys experimentally infected with MV at the early days after infection (Ludlow et al., 2010; Lemon et al., 2011). Instead, MV initiates its infection via SLAM-mediated entry into alveolar macrophages and DCs in the lung or respiratory tracts (de Witte et al., 2008; de Vries et al., 2010; Lemon et al., 2011). These infections may allow MV to penetrate into the human body and reach the lymphoid organs or tissues, where SLAM/CD150-expressing cells are abundant (Corry et al., 1984; Lehmann et al., 2001). After initial replication in these lymphoid organs or tissues, MV or MV-infected lymphocytes can easily enter the bloodstream. Subsequently, a dramatic MV infection is observed in all lymphoid organs, such as the spleen, thymus, appendix, tonsil, and lymph nodes, throughout the body (Moench et al., 1988; Kobune et al., 1996; de Swart et al., 2007; de Vries et al., 2010). At the time when the MV infection of lymphoid organs reaches its peak, MV infection of epithelia, such as squamous stratified epithelia of the tongue and buccal mucosa and ciliated epithelia of the trachea, becomes evident (Nii et al., 1964; Olding-Stenkvist and Bjorvatn, 1976; Moench et al., 1988; de Swart et al., 2007). This epithelial infection is probably led by MV-infected immune cells and initiated through the basolateral side, since monkeys infected with MV often show infectious foci in the epithelia with MV-infected lymphoid or myeloid cells in the subepithelial cell layers of the trachea, bronchus, and tongue (de Vries et al., 2010; Ludlow et al., 2010). The H protein expressed on MV-infected immune cells that migrate through the epithelial cell layer likely recognizes nectin4 expressed at AJs, triggering F protein-mediated membrane fusion between the MV-infected immune cells and the target epithelial cells. Mühlebach et al. (2011) demonstrated a correlation between nectin4 expression and MV infection in epithelia *in vivo*. Importantly, MV has a mechanism that further facilitates virus shedding in the airway. In epithelia, MV selectively releases progeny virus particles from the apical membrane to the luminal side of the respiratory tract (Leonard et al., 2008; Tahara et al., 2008). Leonard et al. (2008) showed that MV genetically engineered to use SLAM/CD150, but not nectin4 (nectin4-blind or SLAM/CD150-tropic), does not shed progeny viruses into the respiratory tract,

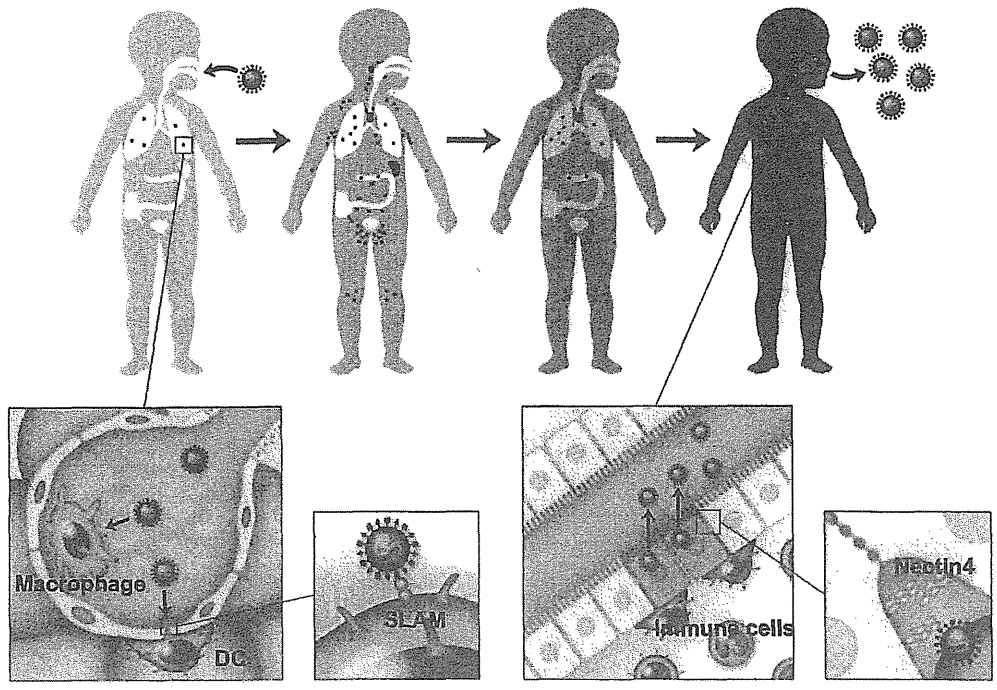

FIGURE 3 | Pathology of measles. MV initiates its infection via SLAM-mediated entry into alveolar macrophages and DCs in the lung. After initial replication in regional lymph nodes, MV enters the bloodstream and subsequently spreads to all lymphoid organs, such as the spleen, thymus, appendix, tonsil, and lymph nodes, throughout the body. When the MV infection of the lymphoid organs reaches its peak, MV-infected immune cells transfer MV to epithelial cells through the basolateral side. At this step, MV uses nectin4 expressed at AJs as a receptor. In the epithelia, MV selectively releases its progeny virus particles from the apical membrane to the luminal side of the respiratory tract.

although it does show systemic infection of lymphoid organs, similar to the case for wt MV.

CONCLUDING REMARKS

Membrane cofactor protein/CD46 was first identified as a receptor for MV (Dorig et al., 1993; Naniche et al., 1993). However, our current knowledge of MV receptors has been totally transformed. In 2000, it was shown that SLAM/CD150 expressed on cells of the immune system, but not MCP/CD46, is a real receptor for wt MV. However, recent studies further showed that SLAM/CD150 is not the sole receptor for MV. MV has an intrinsic ability to enter not only immune cells but also epithelial cells. In 2011, a clear answer was obtained through the identification of the epithelial MV receptor nectin4, which is expressed at AJs, thereby partly explaining why MV exhibits its highly contagious nature (Mühlebach et al., 2011; Noyce et al., 2011). Recent studies on MV receptors greatly advanced our understanding of MV pathogenesis. However, many aspects and molecular mechanisms underlying immunosuppressive effects and a highly contagious nature of MV still remain to be elucidated. Analyses of physiological roles of MV receptors, SLAM/CD150, and nectin4, would provide deep insights into MV pathogenesis.

REFERENCES

Bellini, W. J., Rota, J. S., Lowe, L. E., Katz, R. S., Dyken, P. R., Zaki, S. R., Shieh, W. J., and Rota, P. A. (2005). Subacute sclerosing panencephalitis: more cases of this fatal disease are prevented by measles immunization than was previously recognized. *J. Infect. Dis.* 192, 1686–1693.

Brancati, F., Fortugno, P., Bottillo, I., Lopez, M., Josselin, E., Boudghene-Stambouli, O., Agolini, E., Bernardini, L., Bellacchio, E., Iannicelli, M., Rossi, A., Dib-Lachachi, A., Stuppia, L., Palka, G., Mundlos, S., Stricker, S., Kornak, U., Zambruno, G., and Dallapiccola, B. (2010). Mutations in PVRL4, encoding cell adhesion molecule nectin-4, cause ectodermal dysplasia-syndactyly syndrome. *Am. J. Hum. Genet.* 87, 265–273.

Cannons, J. L., Tangye, S. G., and Schwartzberg, P. L. (2011). SLAM family receptors and SAP adaptors in immunity. *Annu. Rev. Immunol.* 29, 665–705.

Corry, D., Kulkarni, P., and Lipscomb, M. F. (1984). The migration of bronchoalveolar macrophages into hilar lymph nodes. *Am. J. Pathol.* 115, 321–328.

Craighead, J. E. (2000). "Rubeola (Measles)," in *Pathology and Pathogenesis of Human Viral Disease*, ed. J. E. Craighead (Philadelphia, PA: Elsevier Inc.), 397–410.

de Swart, R. L., Ludlow, M., De Witte, L., Yanagi, Y., Van Amerongen, G., Mcquaid, S., Yuksel, S., Geijtenbeek, T. B., Duprex, W. P., and Osterhaus, A. D. (2007). Predominant infection of CD150(+) lymphocytes and dendritic cells during measles virus infection of macaques. *PLoS Pathog.* 3, e178. doi: 10.1371/journal.ppat.0030178

de Vries, R. D., Lemon, K., Ludlow, M., Mcquaid, S., Yuksel, S., Van Amerongen, G., Rennick, L. J., Rima, B. K., Osterhaus, A. D., De Swart, R. L., and Duprex, W. P. (2010). In vivo tropism of attenuated and pathogenic measles virus expressing green fluorescent protein in macaques. *J. Virol.* 84, 4714–4724.

de Witte, L., Abt, M., Schneider-Schaulies, S., Van Kooyk, Y., and Geijtenbeek, T. B. (2006). Measles virus targets DC-SIGN to enhance dendritic cell infection. *J. Virol.* 80, 3477–3486.

de Witte, L., De Vries, R. D., Van Der Vlist, M., Yuksel, S., Litjens, M., De Swart, R. L., and Geijtenbeek, T. B. (2008). DC-SIGN and CD150 have distinct roles in transmission of measles virus from dendritic cells to T-lymphocytes. *PLoS Pathog.* 4, e1000049. doi:10.1371/journal.ppat.1000049

Derycke, M. S., Pambuccian, S. E., Gilks, C. B., Kalloger, S. E., Ghidouche, A., Lopez, M., Bliss, R. L., Geller, M. A., Argenta, P. A., Harrington, K. M., and Skubitz, A. P. (2010). Nectin 4 overexpression in ovarian cancer tissues and serum: potential role as a serum biomarker. *Am. J. Clin. Pathol.* 134, 835–845.

Detre, C., Keszei, M., Romero, X., Tsokos, G. C., and Terhorst, C. (2010). SLAM family receptors and the SLAM-associated protein (SAP) modulate T cell functions. *Semin. Immunopathol.* 32, 157–171.

Devaux, P., Hodge, G., Mcchesney, M. B., and Cattaneo, R. (2008). Attenuation of V- or C-defective measles viruses: infection control by the inflammatory and interferon responses of rhesus monkeys. *J. Virol.* 82, 5359–5367.

Devaux, P., Hudacek, A. W., Hodge, G., Reyes-Del Valle, J., Mcchesney, M. B., and Cattaneo, R. (2011). A recombinant measles virus unable to antagonize STAT1 function cannot control inflammation and is attenuated in rhesus monkeys. *J. Virol.* 85, 348–356.

Dong, Z., and Veillette, A. (2010). How do SAP family deficiencies compromise immunity? *Trends Immunol.* 31, 295–302.

Dorig, R. E., Marcil, A., Chopra, A., and Richardson, C. D. (1993). The human CD46 molecule is a receptor for measles virus (Edmonston strain). *Cell* 75, 295–305.

Fabre, S., Reymond, N., Cocchi, F., Menotti, L., Dubreuil, P., Campadelli-Fiume, G., and Lopez, M. (2002). Prominent role of the Ig-like V domain in trans-interactions of nectins. Nectin3 and nectin 4 bind to the predicted C-C′-C″-D beta-strands of the nectin1 V domain. *J. Biol. Chem.* 277, 27006–27013.

Fabre-Lafay, S., Monville, F., Garrido-Urbani, S., Berruyer-Pouyet, C., Ginestier, C., Reymond, N., Finetti, P., Sauvan, R., Adelaide, J., Geneix, J., Lecocq, E., Popovici, C., Dubreuil, P., Viens, P., Goncalves, A., Charafe-Jauffret, E., Jacquemier, J., Birnbaum, D., and Lopez, M. (2007). Nectin-4 is a new histological and serological tumor associated marker for breast cancer. *BMC Cancer* 7, 73. doi:10.1186/1471-2407-7-73

Griffin, D. E. (2007). "Measles virus," in *Fields Virology*, 5th Edn, eds D. M. Knipe, P. M. Howley, D. E. Griffin, R. A. Lamb, M. A. Martin, B. Roizman, and S. E. Straus (Philadelphia: Lippincott Williams and Wilkins), 1551–1585.

Griffin, D. E., and Ward, B. J. (1993). Differential CD4 T cell activation in measles. *J. Infect. Dis.* 168, 275–281.

Hashimoto, K., Ono, N., Tatsuo, H., Minagawa, H., Takeda, M., Takeuchi, K., and Yanagi, Y. (2002). SLAM (CD150)-independent measles virus entry as revealed by recombinant virus expressing green fluorescent protein. *J. Virol.* 76, 6743–6749.

Jelani, M., Chishti, M. S., and Ahmad, W. (2011). Mutation in PVRL4 gene encoding nectin-4 underlies ectodermal-dysplasia-syndactyly syndrome (EDSS1). *J. Hum. Genet.* 56, 352–357.

Kobune, F., Sakata, H., and Sugiura, A. (1990). Marmoset lymphoblastoid cells as a sensitive host for isolation of measles virus. *J. Virol.* 64, 700–705.

Kobune, F., Takahashi, H., Terao, K., Ohkawa, T., Ami, Y., Suzaki, Y., Nagata, N., Sakata, H., Yamanouchi, K., and Kai, C. (1996). Nonhuman primate models of measles. *Lab. Anim. Sci.* 46, 315–320.

Lehmann, C., Wilkening, A., Leiber, D., Markus, A., Krug, N., Pabst, R., and Tschernig, T. (2001). Lymphocytes in the bronchoalveolar space reenter the lung tissue by means of the alveolar epithelium, migrate to regional lymph nodes, and subsequently rejoin the systemic immune system. *Anat. Rec.* 264, 229–236.

Lemon, K., De Vries, R. D., Mesman, A. W., Mcquaid, S., Van Amerongen, G., Yuksel, S., Ludlow, M., Rennick, L. J., Kuiken, T., Rima, B. K., Geijtenbeek, T. B., Osterhaus, A. D., Duprex, W. P., and De Swart, R. L. (2011). Early target cells of measles virus after aerosol infection of non-human primates. *PLoS Pathog.* 7, e1001263. doi:10.1371/journal.ppat.1001263

Leonard, V. H., Sinn, P. L., Hodge, G., Miest, T., Devaux, P., Oezguen, N., Braun, W., Mccray, P. B., Mcchesney, M. B., and Cattaneo, R. (2008). Measles virus blind to its epithelial cell receptor remains virulent in rhesus monkeys but cannot cross the airway epithelium and is not shed. *J. Clin. Invest.* 118, 2448–2458.

Lightwood, R., and Nolan, R. (1970). Epithelial giant cells in measles as an acid in diagnosis. *J. Pediatr.* 77, 59–64.

Ludlow, M., Rennick, L. J., Sarlang, S., Skibinski, G., Mcquaid, S., Moore, T., De Swart, R. L., and Duprex, W. P. (2010). Wild-type measles virus infection of primary epithelial cells occurs via the basolateral surface without syncytium formation or release of infectious virus. *J. Gen. Virol.* 91, 971–979.

Ma, C. S., and Deenick, E. K. (2011). The role of SAP and SLAM family molecules in the humoral immune response. *Ann. N. Y. Acad. Sci.* 1217, 32–44.

Makhortova, N. R., Askovich, P., Patterson, C. E., Gechman, L. A., Gerard, N. P., and Rall, G. F. (2007). Neurokinin-1 enables measles virus trans-synaptic spread in neurons. *Virology* 362, 235–244.

Moench, T. R., Griffin, D. E., Obriecht, C. R., Vaisberg, A. J., and Johnson, R. T. (1988). Acute measles in patients with and without neurological involvement: distribution of measles virus antigen and RNA. *J. Infect. Dis.* 158, 433–442.

Mühlebach, M. D., Mateo, M., Sinn, P. L., Prufer, S., Uhlig, K. M., Leonard, V. H., Navaratnarajah, C. K., Frenzke, M., Wong, X. X., Sawatsky, B., Ramachandran, S., Mccray, P. B., Cichutek, K., Von Messling, V., Lopez, M., and Cattaneo, R. (2011). Adherens junction protein nectin-4 is the epithelial receptor for measles virus. *Nature* 480, 530–533.

Nakatsu, Y., Takeda, M., Ohno, S., Shirogane, Y., Iwasaki, M., and Yanagi, Y. (2008). Measles virus circumvents the host interferon response by different actions of the C and V proteins. *J. Virol.* 82, 8296–8306.

Naniche, D., Varior-Krishnan, G., Cervoni, F., Wild, T. F., Rossi, B., Rabourdin-Combe, C., and Gerlier, D. (1993). Human membrane cofactor protein (CD46) acts as a cellular receptor for measles virus. *J. Virol.* 67, 6025–6032.

Nii, S., Kamahora, J., Mori, Y., Takahashi, M., Nishimura, S., and Okuno, Y. (1964). Experimental pathology of measles in monkeys. *Biken J.* 6, 271–297.

Noyce, R. S., Bondre, D. G., Ha, M. N., Lin, L. T., Sisson, G., Tsao, M. S., and Richardson, C. D. (2011). Tumor cell marker PVRL4 (nectin 4) is an epithelial cell receptor for measles virus. *PLoS Pathog.* 7, e1002240. doi:10.1371/journal.ppat.1002240

Olding-Stenkvist, E., and Bjorvatn, B. (1976). Rapid detection of measles virus in skin rashes by immunofluroescence. *J. Infect. Dis.* 134, 463–469.

Reymond, N., Fabre, S., Lecocq, E., Adelaide, J., Dubreuil, P., and Lopez, M. (2001). Nectin4/PRR4, a new afadin-associated member of the nectin family that trans-interacts with nectin1/PRR1 through V domain interaction. *J. Biol. Chem.* 276, 43205–43215.

Schneider-Schaulies, S., and Schneider-Schaulies, J. (2009). Measles virus-induced immunosuppression. *Curr. Top. Microbiol. Immunol.* 330, 243–269.

Seki, F., Yamada, K., Nakatsu, Y., Okamura, K., Yanagi, Y., Nakayama, T., Komase, K., and Takeda, M. (2011). The si strain of measles virus derived from a patient with subacute sclerosing panencephalitis possesses typical genome alterations and unique amino acid changes that modulate receptor specificity and reduce membrane fusion activity. *J. Virol.* 85, 11871–11882.

Tahara, M., Takeda, M., Shirogane, Y., Hashiguchi, T., Ohno, S., and Yanagi, Y. (2008). Measles virus infects both polarized epithelial and immune cells by using distinctive receptor-binding sites on its hemagglutinin. *J. Virol.* 82, 4630–4637.

Takai, Y., Ikeda, W., Ogita, H., and Rikitake, Y. (2008a). The immunoglobulin-like cell adhesion molecule nectin and its associated protein afadin. *Annu. Rev. Cell Dev. Biol.* 24, 309–342.

Takai, Y., Miyoshi, J., Ikeda, W., and Ogita, H. (2008b). Nectins and nectin-like molecules: roles in contact inhibition of cell movement and proliferation. *Nat. Rev. Mol. Cell Biol.* 9, 603–615.

Takano, A., Ishikawa, N., Nishino, R., Masuda, K., Yasui, W., Inai, K., Nishimura, H., Ito, H., Nakayama, H., Miyagi, Y., Tsuchiya, E., Kohno, N., Nakamura, Y., and Daigo, Y. (2009). Identification of nectin-4 oncoprotein as a diagnostic and therapeutic target for lung cancer. *Cancer Res.* 69, 6694–6703.

Takasu, T., Mgone, J. M., Mgone, C. S., Miki, K., Komase, K., Namae, H., Saito, Y., Kokubun, Y., Nishimura, T., Kawanishi, R., Mizutani, T., Markus, T. J., Kono, J., Asuo, P. G., and Alpers, M. P. (2003). A continuing high incidence of subacute sclerosing panencephalitis (SSPE) in the Eastern Highlands of Papua New Guinea. *Epidemiol. Infect.* 131, 887–898.

Takeda, M., Kato, A., Kobune, F., Sakata, H., Li, Y., Shioda, T., Sakai, Y., Asakawa, M., and Nagai, Y. (1998).

Measles virus attenuation associated with transcriptional impediment and a few amino acid changes in the polymerase and accessory proteins. *J. Virol.* 72, 8690–8696.

Takeda, M., Tahara, M., Hashiguchi, T., Sato, T. A., Jinnouchi, F., Ueki, S., Ohno, S., and Yanagi, Y. (2007). A human lung carcinoma cell line supports efficient measles virus growth and syncytium formation via a SLAM- and CD46-independent mechanism. *J. Virol.* 81, 12091–12096.

Takeda, M., Takeuchi, K., Miyajima, N., Kobune, F., Ami, Y., Nagata, N., Suzaki, Y., Nagai, Y., and Tashiro, M. (2000). Recovery of pathogenic measles virus from cloned cDNA. *J. Virol.* 74, 6643–6647.

Takeuchi, K., Miyajima, N., Nagata, N., Takeda, M., and Tashiro, M. (2003). Wild-type measles virus induces large syncytium formation in primary human small airway epithelial cells by a SLAM(CD150)-independent mechanism. *Virus Res.* 94, 11–16.

Takeuchi, K., Takeda, M., Miyajima, N., Ami, Y., Nagata, N., Suzaki, Y., Shahnewaz, J., Kadota, S., and Nagata, K. (2005). Stringent requirement for the C protein of wild-type measles virus for growth both in vitro and in macaques. *J. Virol.* 79, 7838–7844.

Tatsuo, H., Ono, N., Tanaka, K., and Yanagi, Y. (2000). SLAM (CDw150) is a cellular receptor for measles virus. *Nature* 406, 893–897.

Veillette, A. (2010). SLAM-family receptors: immune regulators with or without SAP-family adaptors. *Cold Spring Harb. Perspect. Biol.* 2, a002469.

WHO. (2009). Global reductions in measles mortality 2000–2008 and the risk of measles resurgence. *Wkly. Epidemiol. Rec.* 84, 509–516.

Yanagi, Y., Takeda, M., Ohno, S., and Hashiguchi, T. (2009). Measles virus receptors. *Curr. Top. Microbiol. Immunol.* 329, 13–30.

Conflict of Interest Statement: The authors declare that the research was conducted in the absence of any commercial or financial relationships that could be construed as a potential conflict of interest.

Received: 15 November 2011; paper pending published: 26 November 2011; accepted: 26 December 2011; published online: 13 January 2012.

Citation: Takeda M, Tahara M, Nagata N and Seki F (2012) Wild-type measles virus is intrinsically dual-tropic. Front. Microbio. 2:279. doi: 10.3389/fmicb.2011.00279

This article was submitted to Frontiers in Virology, a specialty of Frontiers in Microbiology.

Triggering the measles virus membrane fusion machinery

Melinda A. Brindley[a], Makoto Takeda[b], Philippe Plattet[c], and Richard K. Plemper[a,d,1]

[a]Department of Pediatrics, Emory University School of Medicine, Atlanta, GA 30322; [b]Department of Virology III, National Institute of Infectious Diseases, Tokyo 208-0011, Musashimurayama, Japan; [c]Neurovirology Unit, Division of Experimental Clinical Research, Department of Clinical Research and Veterinary Public Health of the Vetsuisse Faculty, University of Bern, CH-3012 Bern, Switzerland; and [d]Children's Healthcare of Atlanta, Atlanta, GA 30322

Edited by Robert A. Lamb, Northwestern University, Evanston, IL, and approved September 12, 2012 (received for review June 27, 2012)

Paramyxoviruses contain glycoprotein fusion machineries that mediate membrane merger for infection. The molecular framework and mechanistic principles governing receptor-induced triggering of the machinery remain unknown. Using measles virus (MeV) fusion complexes, we demonstrate that receptor binding to only one dimer of the tetrameric attachment protein (H) dimer-of-dimers induces fusion-protein (F) triggering; receptor binding and F triggering can be communicated across the dimer–dimer interface of H; and the physical integrity of the tetramer is maintained during fusion. The central MeV H ectodomain stalk region requires structural flexibility for activation of F, and alanine substitutions in this section, physical stress, or exposure of H to soluble ligands trigger conformational rearrangements in native H tetramers. Binding of soluble receptor to H is sufficient to initiate refolding of F, underscoring the physiological significance of this rearrangement of the H tetramer. These data outline a model of the triggering of the physiological MeV fusion machinery in which unilateral receptor binding to one dimer pair in the H tetramer is sufficient to induce a reorganization of H that affects the conformation of the central stalk section, severing interactions between H and the F trimer and activating refolding of F.

paramyxovirus entry | protein refolding | virus envelope glycoproteins

Enveloped viruses display highly specialized glycoprotein fusion machineries, which, when activated, undergo a series of conformational changes ultimately resulting in membrane merger, fusion pore formation, and infection. All pathogens of the *Paramyxovirinae* subfamily depend on the concerted action of two glycoprotein complexes for infection; the attachment protein (H) binds to the cellular receptor and then activates refolding of the fusion protein (F), which facilitates membrane merger (1). Both proteins are thought to interact specifically in hetero-oligomeric fusion complexes (2–7).

Structural and biochemical studies have advanced our insight into conformational changes in F that are required for fusion (1). In contrast, basic questions about the molecular framework that defines productive receptor binding and the mechanism that links receptor binding to F triggering remain unaddressed: i.e., what is the minimal productive receptor:attachment protein stoichiometry; is receptor immobilization in the target membrane required for triggering of the paramyxovirus fusion machinery; does receptor binding affect the conformation of the attachment protein oligomer, and, if so, is this reorganization of the H tetramer instrumental for F triggering?

Measles virus (MeV), a representative of the *Morbillivirus* genus within the *Paramyxovirinae*, is a paramyxovirus archetype of high clinical significance. We have demonstrated that a homotetramer or higher-order multimer constitutes the physiological oligomer of the MeV H protein (8). Subsequent crystallization of the isolated globular head domains of MeV H complexed with soluble signaling lymphocyte activation molecule (SLAM/CD150) receptor has corroborated this view (9). Like all other *Paramyxovirinae* attachment proteins, the head domain of each MeV H monomer harbors receptor-binding sites (RBS) and assumes the classical β-barrel fold of sialidases, although the H protein lacks neuraminidase activity (9–12). A long stalk domain connects the head of the H protein to the transmembrane domain and short luminal tail. The binding sites for all three reported MeV receptors, CD46, SLAM, and nectin-4 (9, 11, 13), are located in an overlapping area of the head domain (14). MeV H and F complexes are thought to preassemble intracellularly (15), and discrete H stalk residues have been implicated in mediating F protein binding and triggering. Through biochemical analyses of full-length native MeV H fusion complexes, we have identified residues in the central section of the stalk domain (position 111–118) that, when mutated, prevent physical association of H and F. Position 98 in the H stalk, slightly more membrane proximal, was shown to be required for efficient triggering of F (16). Having developed an MeV H bimolecular complementation (H-BiC) assay, we furthermore demonstrated that the RBS, F-interacting, and F-triggering functionalities are truly distinct. Coexpression of H mutants with functional defects in these domains restores fusion-support activity through transcomplementation (8, 17).

The structure of the attachment protein stalk domains remains to be solved in its entirety, but the crystal structures of soluble Newcastle disease virus (NDV) hemagglutinin-neuraminidase (HN) attachment protein head and partial stalk domains show a four-helix bundle (4HB) organization of the stalk (18). This arrangement was corroborated by the structure of the parainfluenza virus type 5 (PIV5) HN stalk (19), suggesting that a 4HB stalk arrangement is conserved among *Paramyxovirinae* attachment proteins.

Crystal structures of free and receptor-bound isolated H head domains in monomeric, dimeric, or tetrameric configurations have revealed that the fold of individual head monomers and the organization of the monomer–monomer interface in covalently linked H dimers remain largely unchanged upon receptor binding (9–12). By contrast, tetrameric ectodomain fragments of both H- (9) and related HN-type (18, 20) attachment proteins crystallized in different spatial organizations. For H, these structures were speculated to represent pre- and postreceptor bound/F-triggering conformations. However, the physiological relevance of individual conformations of purified H ectodomain fragments and the question of whether receptor binding induces a reorganization of the attachment protein remain unaddressed.

Building on available structural and functional information and using an array of newly established functional assays, the present study identifies fundamental determinants that link H

Author contributions: M.A.B. and R.K.P. designed research; M.A.B. and R.K.P. performed research; M.A.B., M.T., P.P., and R.K.P. contributed new reagents/analytic tools; M.A.B., M.T., P.P., and R.K.P. analyzed data; and M.A.B. and R.K.P. wrote the paper.

The authors declare no conflict of interest.

This article is a PNAS Direct Submission.

[1]To whom correspondence should be addressed. E-mail: rplempe@emory.edu.

See Author Summary on page 17750 (volume 109, number 44).

This article contains supporting information online at www.pnas.org/lookup/suppl/doi:10.1073/pnas.1210925109/-/DCSupplemental.

receptor engagement to F triggering. Cysteine engineering combined with the H-BiC assay defined the molecular framework of H tetramer–receptor interactions that are necessary for fusion triggering. Insertion of disulfide bonds at strategic positions probed the physiological relevance of existing structural models of the H tetramer, and biochemical and functional assays explored the effect of soluble and membrane-embedded receptor on the H tetramer and associated F trimer organization under physiological conditions.

Results

We have shown previously that bioactivity of MeV H mutants with discrete functional defects (illustrated in Fig. 1*A*) can be restored through protein transcomplementation after coexpression (8). This H-BiC assay provides a platform to explore individual H functionalities in the context of physiological, membrane-embedded fusion complexes. However, the approach is limited by an inherent inability to differentiate between complementation on a heterodimer or [which presumably would be more informative based on recent structural information (9)] on a homodimer/heterotetramer level. To explore transcomplementation across the dimer–dimer interface in H homodimer/heterotetramers complementation pairs, we hypothesized that the two natural disulfide bonds at H stalk positions 139 and 154, which mediate covalent H dimerization, could be used in a combination of H-BiC with disulfide bond engineering (Fig. 1*B*).

MeV H Heterodimers with Unpaired Stalk Thiols Are Intracellularly Retained. Previously, we have demonstrated that substituting either cysteine 139 or cysteine 154 with serine retains H bioactivity (21). We therefore anticipated that coexpression of standard H with H-C139S will result in the formation of H-H and (H-C139S)-(H-C139S) homodimers that are fully intracellularly transport competent because of the pairing of all reactive thiol moieties present in the ectodomains. In contrast, H-(H-C139S) heterodimers are expected to be intracellularly retained by endoplasmic reticulum (ER)-resident isomerases that target unpaired, reactive thiol groups (22). H variants harboring HA or Flag epitope tags for distinction were generated to test this hypothesis conceptually in coimmunoprecipitation experiments of cell-surface–exposed and total H material.

H_{HA}-H_{FLAG} complexes were present in both whole-cell extracts and the plasma membrane fractions. However, plasma membrane levels of H_{HA}-(H-C139S_{FLAG}) heterodimers were greatly reduced (Fig. 1*C*), demonstrating that disulfide engineering is suitable to control the composition of H tetramers in surface-exposed, functional fusion complexes. Equivalent results were obtained with H variants featuring the C139S substitution in addition to one of the signature mutations of the different complementation groups, i.e., F111A, which affects F interaction (6); ΔCD46, which affects receptor binding (23, 24); or I98A, which affects F triggering; Fig. 1*C* (16).

Unilateral Receptor Engagement by a Single Dimer of the H Tetramer Is Sufficient for F Triggering. To explore whether transcomplementation of the individual H functionalities can be achieved in a homodimer/heterotetramer setting, we coexpressed H complementation variants pairwise in all combinations with MeV F and quantified bioactivity using a luciferase reporter-based cell-to-cell fusion assay. Efficient complementation, similar to that seen with the H-C139S reference, was observed upon combination of H-I98A-C139S with H-ΔCD46 (Fig. 2 and Fig. S1). In contrast, F-triggering activity was not restored when we paired F-interaction–deficient H-F111A homodimers with homodimers of either of the other two complementation groups. Naturally, the C139S substitution itself did not restore the triggering competence of any of the H mutants when expressed with F alone for control.

These results indicate that unilateral receptor binding to only one of the covalently linked dimer pairs in the attachment protein tetramer is sufficient for F triggering. Unlike efficient compensation of the H-F111A substitution in a heterodimer setting (8), however, F-binding–deficient H-F111A homodimers cannot be complemented *in trans*.

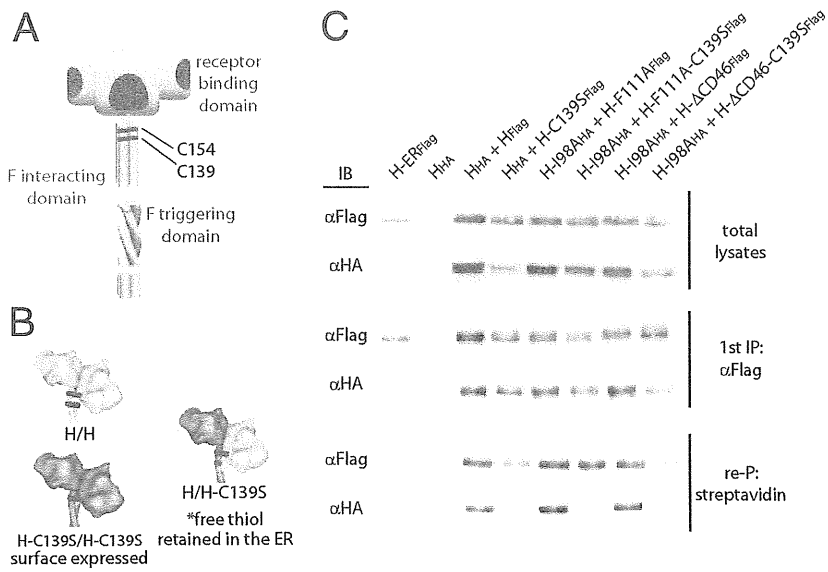

Fig. 1. Cysteine engineering to assess selective H transcomplementation on a homodimer/heterotetramer level. (*A*) Schematic of the MeV H tetramer; the locations of independent complementation groups and naturally present disulfide bonds are indicated. (*B*) Illustration of the cysteine-engineering strategy. (*C*) Coimmunoprecipitation of epitope-tagged surface-exposed H dimers confirms that only H homodimers with paired thiol moieties reach the cell surface. Surface proteins were biotinylated, and total cell lysates were subjected to α-Flag immunoprecipitation (first IP), followed by reprecipitation (re-P) of the plasma membrane fraction with immobilized streptavidin. A previously described H variant carrying an endoplasmic reticulum-retention signal (H-ER_{Flag} (15)] served as specificity control for the streptavidin reprecipitation. Immunoblots were developed with α-Flag or α-HA antibodies, respectively.

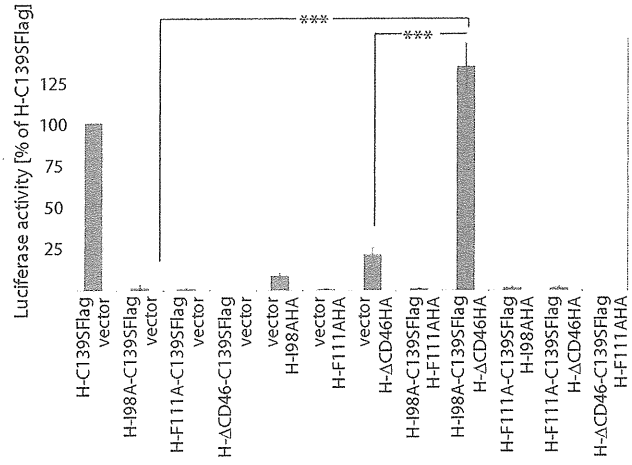

Fig. 2. Unilateral interaction of a receptor with a single covalently linked H dimer is sufficient to initiate F triggering. Results of a quantitative firefly luciferase-based cell-to-cell fusion assay assessing H transcomplementation are shown; data represent averages of at least four experiments ± SEM; ***$P < 0.001$.

Distinct Conformations of Attachment Protein Tetramers. Two distinct scenarios could account for this lack of trans-complementation: Heterotetramers containing H-F111A homodimers could form physically but lack functionality, suggesting that each covalent dimer pair must contain at least one F-binding–competent H monomer. Alternatively, H-F111A homodimers may be unable to associate into heterotetramers with either H-I98A or H-ΔCD46 homodimers, implying that they assume a conformation that is competent for intracellular transport but conformationally distinct from either H-I98A or H-ΔCD46.

To differentiate between these possibilities, we generated a set of electrophoretically distinct H variants by adding single-chain antibody moieties as size tags to the H C terminus as reported previously (25). Adding single or tandem copies of the single-chain antibody resulted in H_{XL} and H_{XXL} constructs, respectively, with an estimated increase of ~25 kDa per single-chain antibody copy, largely unchanged bioactivities (Table S1), but clearly distinguishable electrophoretic mobility (Fig. S2*A Upper*). Electrophoretic separation of surface-expressed material after coexpression of standard and size-tagged H constructs under denaturing, nonreducing conditions underscored that heterodimers form readily but that heterodimers harboring an unpaired thiol moiety at position 139 are not competent for intracellular transport (Fig. S2*A Lower*), confirming that the added single-chain domain does not affect the homodimer engineering strategy.

We next subjected the size-tagged H_{XXL} constructs to digitonin extraction followed by native-PAGE, which fractionates the intact H tetramers according to mass, shape, and surface charge (8, 26). When standard and size-tagged variants of otherwise unmodified H, H-I98A, and H-ΔCD46, all with and without the C139S substitution, were coexpressed, tetramers of intermediate mobility representing mixed homodimer/heterotetramers complexes became readily appreciable in addition to untagged and size-tagged homotetramers (Fig. 3*A*). However, H homodimers harboring the F111A mutation failed to engage in mixed tetramers with standard H, H-I98A, or H-ΔCD46-dimers (Fig. 3*A*), suggesting that H-F111A tetramers have a distinct conformation. Fig. S2*B* summarizes the complementation and oligomerization phenotypes of all H constructs analyzed in an activity matrix.

Under native-PAGE conditions, conformational rearrangements that result in a change of protein shape and/or surface charge typically are reflected by an altered mobility pattern (27, 28). Indeed, direct comparison of standard H and representatives of the different H complementation groups without additional size tags revealed two distinct banding patterns: tetramers of all H mutants that are confirmed to abrogate physical interaction with F [i.e., H-F111A, H-L114A, H-I118A, and an H-110–114A quintuple mutant (6)] were found predominantly in a fraction of higher electrophoretic mobility than those of standard H, F-triggering–, or receptor-binding–defective H variants (Fig. 3*B Upper*). A small fraction of H-F111A, H-L114A, and H-I118A found at higher molecular weight may represent higher-order oligomers or protein aggregates. Standard reducing and denaturing SDS/PAGE of the same samples confirmed that the underlying H monomers are all of equivalent molecular weight (Fig. 3*B Lower*). Because the overall protein pI is unaffected by the amino acid substitutions introduced at H positions 111, 114, or 118, the altered native-PAGE mobility pattern indicates a different conformation of the F-binding–deficient H tetramers that is distinct from that of standard H, H-I98A, and H-ΔCD46.

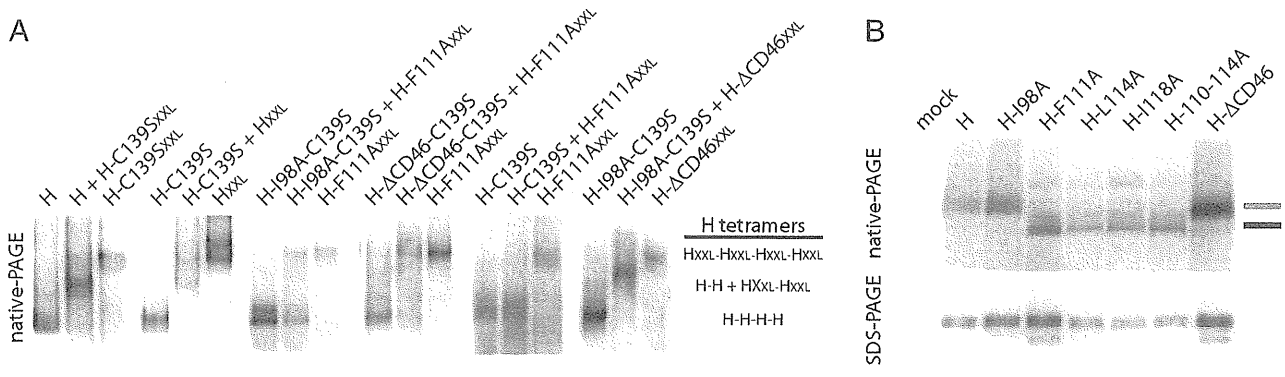

Fig. 3. H-F111A homodimers are structurally distinct from homodimers of unmodified H or other H-complementation groups. (*A*) Native-PAGE analysis of digitonin-extracted H tetramers reveals that H-F111A homodimers are unable to heterotetramerize with any other H homodimer species. To distinguish better untagged and size-tagged H oligomers in native-PAGE, size-increased H constructs contained a tandem copy of the tag H_{XXL}. The migration positions of size-tagged H homo- and heterotetramers are shown. (*B*) H homotetramers harboring stalk mutations that prevent interaction with F (F111A, L114A, I118A, or 110-114A) show a distinct migration pattern in native gels. The predominant H tetramer migration profiles of standard H, H-I98A, and H-ΔCD46 (gray marker) and H-F111A (black marker) are shown.

Induced Rearrangement of the H Tetramer into an H-F111A–Like Conformation. To test the physiological relevance of the different H tetramer organizations, we examined whether standard H tetramers can rearrange into an H-F111A–like conformation. We first explored the effect of increasing detergent stringency or temperature shock on the organization of H tetramers. n-Dodecyl β-D-maltoside (DDM) is, like digitonin, a nonionic detergent used for native-PAGE (26), but in our experience it applies higher scrutiny to larger protein complexes such as the MeV H tetramer (8). Adding increasing amounts of DDM to digitonin-extracted H tetramers reliably converted the standard H and H-I98A tetramer mobility pattern to the H-F111A profile (Fig. 4*A*). Consistent with our previous observations (8), H tetramers partially disintegrated into the covalently linked dimers at higher DDM concentrations.

Heat exposure has been used to trigger refolding of purified paramyxovirus F proteins into the postfusion conformation (29). When we subjected the MeV H complexes in an analogous experimental approach to brief (10-min) heat treatment followed by native-PAGE, we noted predominant reorganization of standard H and H-I98A tetramers into an H-F111A–like configuration at or above 50 °C (Fig. 4*B*), comparable to the conformational shift observed in the presence of increasing DDM concentrations.

Proteinaceous Ligands Induce H Tetramer Reorganization. To assess further the relevance of detergent or heat-induced H tetramer rearrangements, we next exposed the panel of H variants to purified, soluble SLAM receptor (sSLAM) (Fig. 5*A*) (6) or a neutralizing monoclonal antibody (mAb E128) that recognizes an epitope located in the CD46 RBS (Fig. 5*B Upper*), followed by digitonin extraction and native-PAGE. After the addition of sSLAM or RBS-specific mAb, the electrophoretic mobility of H oligomers was reduced, indicating the formation of larger H tetramer-sSLAM and H tetramer-mAb complexes. Importantly, the mobility profile of all three H variants (standard H, H-I98A, and H-F111A) became similar when complexed with sSLAM or RBS-specific mAb. In contrast, the difference in mobility between H-F111A and standard H or H-I98A remained when a nonneutralizing α-MeV H mAb mixture was added for comparison (Fig. 5*B Lower*). sSLAM and the different mAbs displayed similar electrophoretic mobility in native-PAGE when fractionated in the absence of H complexes (Fig. S3*A*), and an H-ΔCD46 variant that is not recognized by mAb E128 (Fig. S3*B*) confirmed the specificity of the mAb E128–H interaction (Fig. 5*B*).

To address whether gel shifts induced through physical stress (heat shock or stringent detergent extraction) and through the addition of protein ligands (sSLAM or α-RBS mAb) visualize equivalent rearrangements of the H tetramer, we examined the effect of heat shock and exposure to ligand in combination. If either procedure induced H tetramer rearrangements of the same molecular nature, we would expect to extract H complexes with mobility equal to that of complexes exposed to soluble ligand alone. This was indeed the case when gel shift assays were performed after consecutive exposure of standard H tetramers to heat and/or proteinaceous (sSLAM or mAb E128) ligands (Fig. 5*C*). These data indicate that standard H tetramers can rearrange into an H-F111A–like conformation and suggest that binding of proteinaceous ligands (either soluble receptor or RBS-specific mAbs) to H is sufficient to trigger this reorganization.

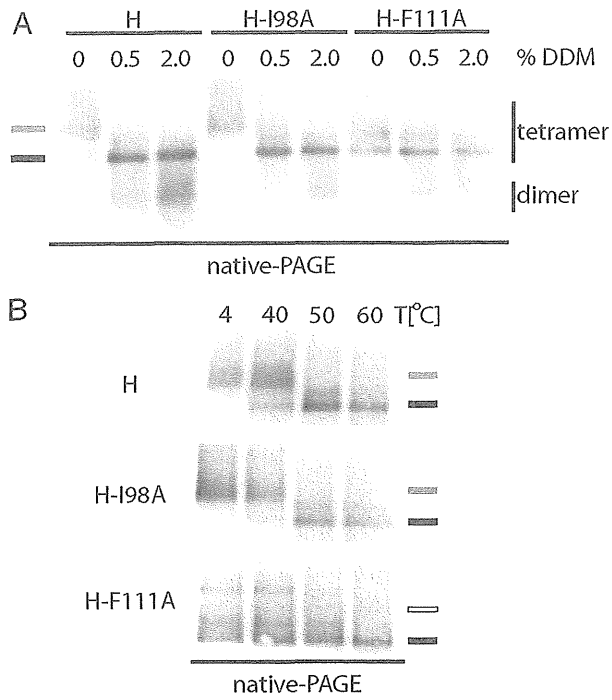

Fig. 4. Physical stress induces transition of H tetramers to an H-F111A–like conformation. (*A*) Digitonin extracts of H tetramers were treated with increasing amounts of DDM and subjected to native-PAGE fractionation. The predominant tetramer migration profiles as observed in Fig. 3*B* are shown. (*B*) Digitonin extracts of H tetramers were subjected to 10-min heat treatment before native-PAGE analysis.

Upper H Stalk Sections Retain a Closed Arrangement During F Triggering. Different conformations of H oligomers appear consistent with the two distinct tetrameric crystal structures that were reported recently for soluble MeV H head domains complexed with SLAM receptor (9). Of these, a predicted pre-F triggering conformation (form I) posits the H stalk domains in a 4HB arrangement, compatible with that observed in NDV and PIV5 HN stalk structures (18, 19). In contrast, a second structure (form II) that was suggested to represent a postreceptor-bound/F-triggering organization of the H tetramer features discrete H stalk dimers. The transition of H from form I to form II was predicted to coincide with the separation of the membrane-distal stalk sections (9).

Fig. 6*A* provides a homology model of the central MeV H stalk section that we generated based on the PIV5 HN coordinates. The model positions residues 98, involved in F triggering (16), and 111 flanking a predicted transition from a twisted to a straight 4HB arrangement. Based on the inability of H-F111A tetramers to interact with F, we considered that the higher H-F111A–like mobility may represent a form II-like structural organization. To test the relevance of form II experimentally, we inserted cysteine substitutions at selected positions along the length of the H stalk. The resulting H variants were assayed first for intracellular transport competence (Table S1) and the formation of covalently linked tetramers assessed through electrophoretic fractionation under reducing and nonreducing conditions (Fig. 6*B*). Two of the constructs, H-K72C and H-I122C, were not surface expressed, presumably because of the presence of unpaired thiol moieties in the stalk. Of the remaining, intracellular transport-competent mutants, four H variants (H-L114C, H-Y131C, H-D132C, and H-D151C) exist predominantly (>50%) as covalently linked tetramers (Fig. 6 *B* and *C*).

When we assessed the bioactivity of these constructs in quantitative fusion assays, no clear correlation between covalent H tetramerization and fusion-triggering activity was observed. The three H variants that showed the highest degree of covalent tetramers (H-Y131C, H-D132C, and H-D151C) were all capable of robust F triggering, ranging from ~60–120% of that found for standard H (Fig. 6*C*). These data indicate that the molecular integrity of preformed H tetramers is conserved during F triggering and reveal the consistently maintained close proximity of the

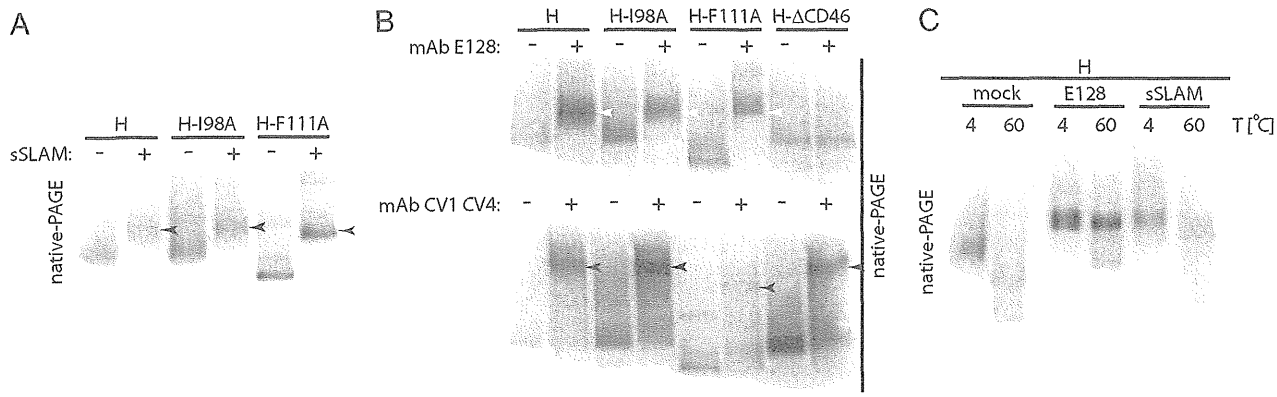

Fig. 5. RBS-specific soluble ligands induce H tetramer reorganization. (*A*) Exposure of H-expressing cells to sSLAM before digitonin extraction and native-PAGE analysis returns H tetramer/sSLAM complexes of similar mobility (arrowheads). (*B*) Exposure of H-expressing cells to RBS-specific mAb E128 (competes with CD46 receptor binding) or nonneutralizing H-specific mAbs CV1 CV4. Although all E128/H tetramer complexes show indistinguishable migration profiles (white arrowheads), CV1 CV4/H-F111A tetramers retain distinct electrophoretic mobility (black arrowheads). (*C*) Consecutive exposure of H tetramers to heat and RBS-specific ligands. H material was extracted with digitonin and was kept at 4 °C (4) or was heated to 60 °C (60) for 10 min. Subsequently, samples were exposed to RBS-specific ligand (E128, sSLAM) or vehicle (mock).

membrane-distal (upper) stalk sections in pre- and postreceptor-bound H complexes.

F Triggering Requires Structural Freedom in the Central Section of the H Stalk. If the F111A mutation indeed induces a postreceptor-bound–like organization of H, this finding implies that the conformation of H-F111A tetramers should be distinct from that of crystal form II. To test this notion, we examined whether H-F111A variants remain capable of forming covalently linked tetramers when cysteine substitutions are added to stalk positions membrane proximal or distal of the F111A site (i.e., positions L74C, Y131C, D132C, or D151C). Comparative analysis of

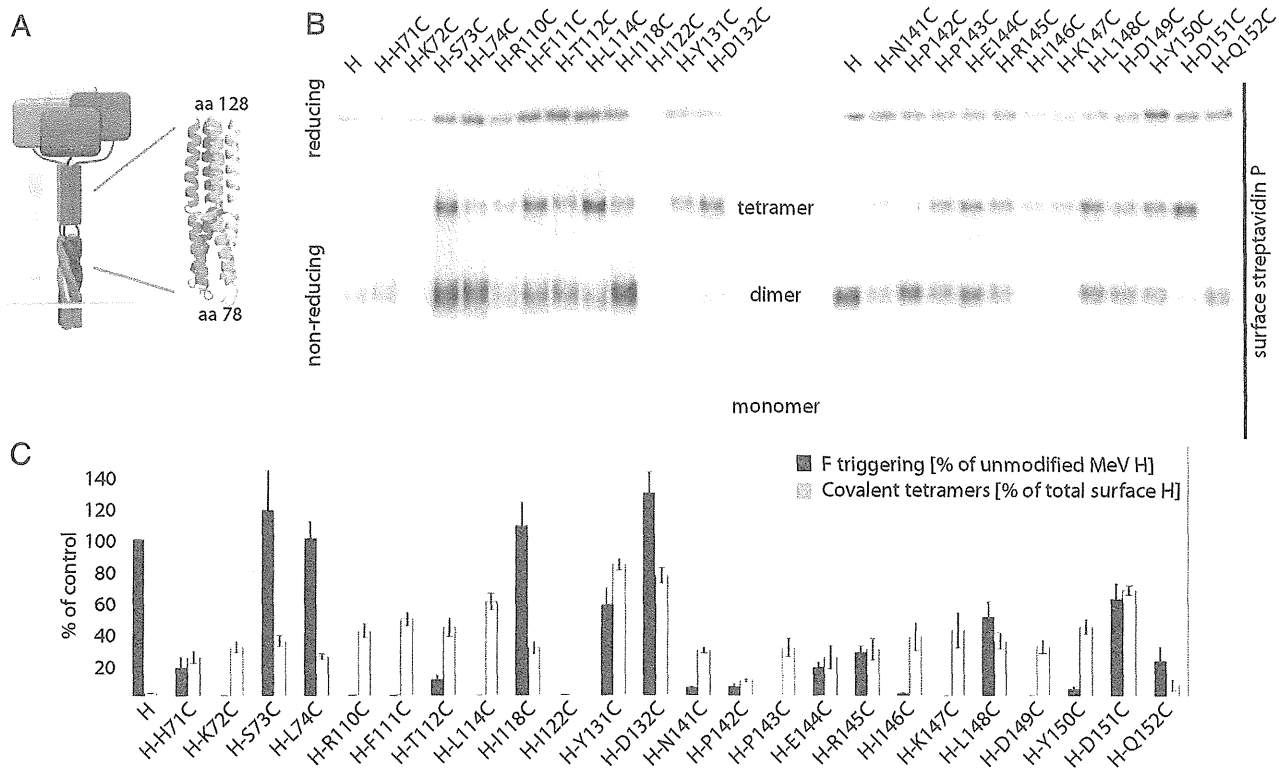

Fig. 6. Membrane-distal (upper) H stalk sections maintain close physical proximity during F triggering. (*A*) Overview of the cysteine-scanning mutagenesis performed along the H stalk, represented by a yellow bar (*Left*) in the cartoon. (*Inset*) Homology model of the central section of the MeV H stalk, generated in Swiss-MODEL based on the coordinates of a PIV5 HN stalk fragment (PDB ID 3TSI). (*B*) Assessment of the covalent oligomerization status of cell-surface–exposed H cysteine mutants under reducing and nonreducing conditions. (*C*) Quantitation of relative amounts of surface-exposed H in covalent tetramers (based on densitometric analysis of gels as shown in *B*) and F-triggering activity; data represent average of four experiments ± SEM.

these constructs with the corresponding single mutants under reducing and nonreducing conditions demonstrated that the F111A exchange does not affect the degree of covalent H tetramerization (Fig. 7*A*). Of note, combining distal cysteine insertions with removal of the naturally existing disulfide bonds at stalk positions 139 or 154 abrogates essentially all covalent H tetramerization (Fig. 7*B*), indicating that the natural disulfide bonds at positions 139 and 154 introduce a rigid scaffold into the dimeric stalk pairs that is required for covalent tetramerization.

In contrast to the high bioactivity of H tetramers with covalently rigidified upper-stalk sections, cysteine substitutions introduced into the central part of the stalk itself (residues 110, 111, 112, and 114) largely blocked F triggering (Figs. 6C and 7C). An exception was H-118C, which maintained efficient fusion support activity. Consistent with this finding, H-118C, but not H-118A, is able to associate efficiently with F (Fig. S4), underscoring the highly specific side-chain requirement in the H stalk section for productive F binding. However, when we partially released disulfide bonds of H-110C, H-111C, H-112C, and H-114C under mildly reducing conditions [25 mM dithiothreitol (DTT)], the bioactivity of all variants except H-114C was restored substantially, to ~60–85% of that observed for standard H (Fig. 7*C*). This finding is consistent with our recent analysis of the homologous region of the related canine distemper virus H protein (30), suggesting that structural, possibly rotational, freedom between stalk monomers in a central, but not upper, stalk section is a conserved requirement for morbillivirus F triggering. Although additional disulfide bonds near stalk position 111 arrest H-F111C tetramers in a reactivatable, pre–F-triggering organization, the conformation of H-F111A tetramers may represent a distinct postreceptor-bound/F-triggering form of the tetramer.

Exposure of H Tetramers to Soluble Receptor Initiates F Trimer Refolding. To test directly whether the H-F111A tetramer conformation represents a post-F-triggering form, we examined the effect of soluble receptor-induced H tetramer rearrangements on the initiation of F triggering in physiological, membrane-embedded fusion complexes. To detect the initiation of F trimer refolding, we used a pair of mAbs directed against the MeV F protein, mAb 186A (31) and, mAb 19GD (32), which we have found specifically detect a pretriggered (α-pre F) or a fusion-triggered (α-trig F) conformation of the F trimer, respectively (Fig. 8*A*).

To generate conditions void of high-affinity receptor stimulation of H, CD46-binding– incompetent H-ΔCD46 and F were coexpressed in Vero cells, which lack both SLAM and nectin-4 (9, 13) and therefore do not provide a receptor for H-ΔCD46. In this system, we observed strong reactivity of F trimers with the pretriggered F-specific mAb in cell-surface immunoprecipitation assays, whereas the corresponding α-triggered F-specific mAb showed little binding (Fig. 8*B*). Likewise, F expressed in the absence of H maintained full reactivity with the pretriggered F-specific mAb. These data indicate that prefusion MeV F trimers have a low rate of spontaneous refolding in the absence of H interaction with receptor and demonstrate that MeV F does not require physical contact with H to retain a metastable prefusion conformation.

When MeV glycoprotein-expressing cells were exposed to soluble SLAM, however, reactivity with the α-triggered F mAb increased substantially to levels comparable to those achieved through overlay with SLAM-positive Vero-SLAM cells, which served as a positive control for the assay (Fig. 8*B*). Corroborating previous reports that the I98A substitution in the H stalk impairs F triggering but not physical interaction between H and F complexes (8, 16), exposure of H-I98A tetramers to membrane-integral or soluble receptor in this experimental setting did not result in increased F reactivity with the α-triggered F mAb (Fig. S5*A*).

To explore whether the soluble SLAM-mediated initiation of F triggering is sufficient to drive the opening of fusion pores, we adapted a recently described real-time cell-content–mixing assay to the paramyxovirus system; this assay is based on the functional reconstitution of individually expressed N- and C-terminal halves of GFP/renilla luciferase dual-fusion proteins upon the formation of fusion pores (33). Monitoring the reconstitution of functional luciferase moieties in this setting revealed successful opening of fusion pores only in the presence of membrane-integral receptor (Fig. 8*C*). Low-level content mixing observed with the H-ΔCD46 and F combination in the absence of soluble SLAM is most likely caused by residual low-affinity docking of H-ΔCD46 to the CD46 receptor. Importantly, exposure of Vero cell populations expressing H-ΔCD46 and F to soluble SLAM did not

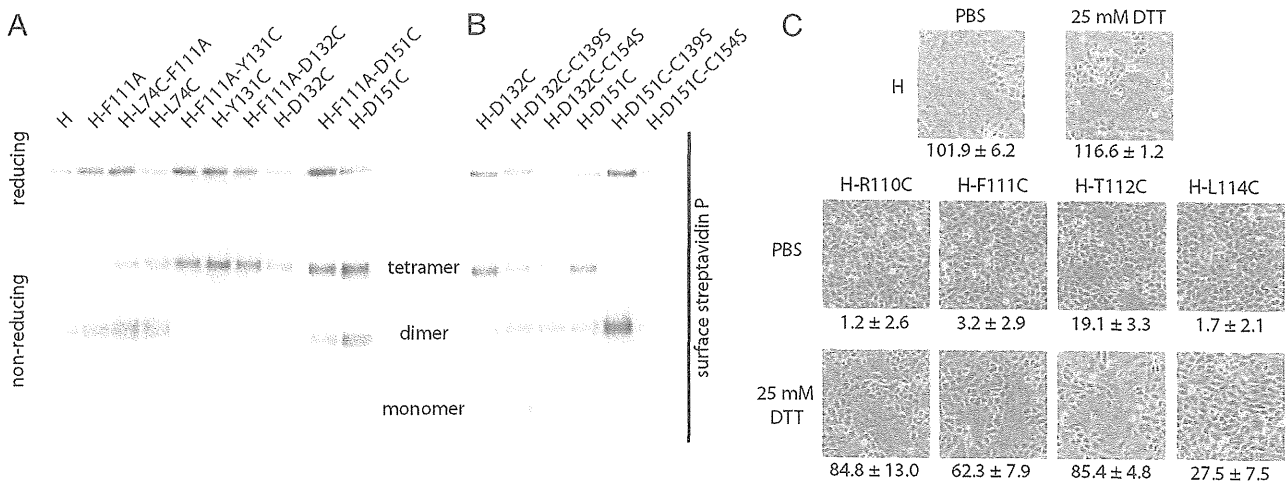

Fig. 7. Structural flexibility of the central section of the H-stalk domain is required for F triggering. (*A* and *B*) Assessment of the covalent oligomerization status of selected H cysteine mutants. (*C*) Microphotographs of Vero cells coexpressing MeV H constructs with standard F protein. Before imaging, cells were exposed to mildly reducing conditions (25 mM DTT) or vehicle (PBS) for control. Numbers represent the amount of nuclei found in a syncytia/standardized field of view (each control field contains ~100–120 cells). Averages of 75 fields of view ± SEM are shown.

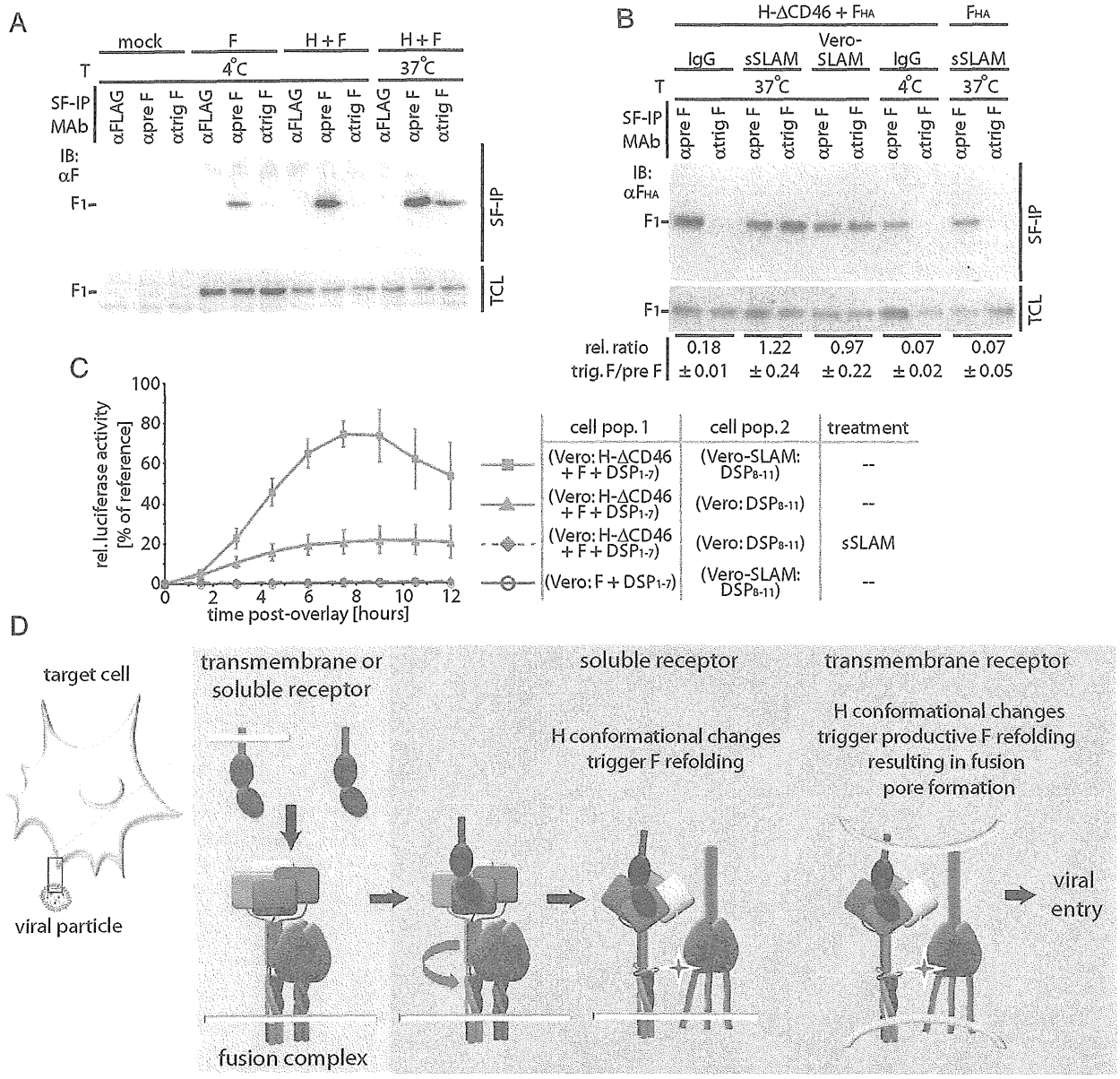

Fig. 8. H tetramer conformational changes induced by soluble receptor are sufficient to initiate F refolding. (*A*) Surface immunoprecipitation (SF-IP) of Vero cells coexpressing MeV H and F. Precipitation of F material with a conformation-dependent mAb that recognizes a fusion-triggered F trimer (αtrig F) requires warming of samples to 37 °C, allowing F refolding to proceed. A mAb recognizing prefusion F (αpre F), and a control mAb (αFlag) were used for comparison. (*B*) Surface immunoprecipitation of MeV F protein with conformation-dependent αpre F and αtrig F mAbs as specified. Overlay of MeV SLAM receptor-positive cells (Vero-SLAM) or sSLAM is sufficient to initiate F refolding. Numbers represent densitometric ratios of triggered F/prefusion F, normalized for F material present in total cell lysates (TCL); averages of three experiments ± SEM are shown. (*C*) Initiation of F refolding by soluble receptor does not lead to fusion pore formation. Values were normalized for cells cotransfected with DSP_{1-7} and DSP_{8-11} plasmids (33) and represent averages of four to six experiments ± SEM. (*D*) Model of the MeV fusion machinery. Contact of a single H dimer present in functional fusion hetero-oligomers (light blue background; H tetramers are colored by monomer; F trimers are in dark blue) with membrane-embedded or soluble receptor leads to reorganization of the central H stalk section (red arrow); this reorganization most likely coincides with rearrangements of the H head domain. This H tetramer reorganization triggers the F refolding cascade. However, interaction of H with membrane-embedded receptor is required for productive membrane fusion.

lead to increased cell content mixing and syncytia formation in this assay or upon microscopic examination (Fig. S5*B*).

These studies demonstrate that binding of soluble receptor molecules to a native, membrane-embedded paramyxovirus attachment protein oligomer is sufficient to activate the F refolding pathway, suggesting that the ligand-induced changes in H electrophoretic mobility in native gels reflect an H tetramer reorganization that constitutes the central link between binding to a receptor and triggering of the F fusion machinery. Opening of fusion pores, however, requires the presence of membrane-embedded receptor.

Discussion

Paramyxoviruses depend on the concerted action of two envelope glycoprotein complexes to achieve membrane fusion and infection. In this study, we subjected full-length, membrane-

integral MeV attachment protein complexes to an array of biochemical and functional assays to dissect the molecular mechanism that links receptor engagement by the H protein to F-triggering under physiological conditions.

From H transcomplementation assays (8) combined with cysteine-substitution–based homodimer engineering, we conclude, first, that an H monomer:receptor stoichiometry $\leq$2:1 initiates fusion and that unilateral receptor docking to only one of the covalently linked dimer pairs in the H tetramer is necessary and sufficient. Based on these results, we can exclude triggering models that assume separation of the tetrameric H head arrangement along the noncovalent dimer–dimer interface as a result of physical force generated through simultaneous binding of membrane-immobilized receptor molecules to each covalent dimer pair. However, productive complementation across cysteine-engineered F-triggering– or receptor-binding–defective H homodimers reveals functional cross-talk along the dimer–dimer interface.

The generation of triggering-competent covalently linked H tetramers through disulfide bond engineering into the upper (membrane-distal) stalk domain indicates that the molecular integrity of the tetramer itself remains unchanged during receptor binding and F triggering. Thus, efficient F triggering does not mandate complete separation of a tetrameric H stalk assembly, as proposed for an alternative H tetramer-SLAM cocrystal arrangement (form II in ref. 9). Rather, our study suggests that MeV H stalks form a single bundle, consistent with the recently described partial ectodomain structures of NDV (18) and PIV5 (19) HN proteins, and that F triggering does not mandate altering the overall integrity of this organization.

However, efficient F triggering requires structural flexibility between individual H monomers in the central section of the stalk bundle. Cysteine substitutions in this region (residues 110–114) completely abolish fusion-support activity, independent of whether the substitutions induce covalent tetramers or lead to an additional disulfide bond between monomers of an existing covalent H dimer. Considering our experience that unpaired stalk thiols result in intracellular retention of the protein, we assume that the engineered stalk cysteines are engaged in novel disulfide bonds. Confirmation for this notion comes from our observation that exposure of H-110C, H-111C, and H-112C complexes to reducing conditions partially restored fusion-support activity. This finding also demonstrates that the engineered disulfide bonds trap the H tetramer in a pre–F-triggering conformation. In contrast, disulfide bonds at position 114 inhibited fusion activation, even under reducing conditions. Because this variant also was fully intracellular transport competent, gross protein misfolding is unlikely. Alternatively, H-114C may assume a post–F-triggering–like conformation, or this substitution may impair interaction with F on a short-range basis.

Our successful previous engineering of N-linked glycans into consecutive positions (110-112) of the MeV H stalk highlights that each monomer enjoys a high degree of rotational freedom in this region (6). This flexibility is accentuated further by a modeling-predicted disturbance in the secondary structure of the monomers immediately upstream of residue 110. We postulate that local unraveling or rotational unwinding involving the central sections of each stalk monomer is required for F triggering (visualized schematically in Fig. 8*D*). Likewise, the stalk domains of the attachment proteins of many *Paramyxovirinae* subfamily members were implicated in F triggering (2, 16, 34). Our recent analysis of the related canine distemper virus H stalk domain (30) revealed a comparable requirement for structural freedom of the stalk center, suggesting a common theme of *Paramyxovirinae* attachment-protein–mediated fusion support.

The homodimer/heterotetramer complementation studies and native-PAGE assays prove that receptor binding induces biochemically appreciable conformational changes in the H tetramer. H homodimers harboring alanine substitutions in the central stalk section spontaneously assume an organization distinct from that of wild-type H dimers. They homotetramerize efficiently but are incapable of F binding (6) and are unable to associate into heterotetramers with standard H or any of the other complementation groups. However, exposure to physical stress, soluble receptor, or mAbs mimicking receptor binding through interaction with the RBS is sufficient to initiate the reorganization of standard H tetramers into an H-F111A-like conformation, suggesting that the latter may represent a final, postreceptor-binding/F-triggering structure. This hypothesis is substantiated by our demonstration that exposure to soluble receptor is sufficient to initiate F refolding in native, membrane-embedded paramyxovirus fusion complexes. The significance of this finding is threefold: It underscores the physiological significance of the H tetramer rearrangement observed in native-PAGE assays; it demonstrates that little external energy is required to trigger the *Paramyxovirinae* entry cascade; and it confirms that triggering is achieved readily at the plasma membrane under neutral pH conditions.

We note that, upon exposure to physical stress or soluble receptor, the F-triggering–defective H-I98A tetramers also undergo a conformational rearrangement resembling that of standard H tetramers. Previous studies have revealed a substantially higher F coimmunoprecipitation efficiency with H-I98A than with unmodified H; this finding was interpreted as indicating a stronger physical interaction of H-I98A F glycoprotein oligomer pairs (16). Our results may reflect that receptor binding to H-I98A is insufficient to induce the H tetramer rearrangements because of a stabilizing effect of tightly bound F. Alternatively, the H-I98A substitution could impair the separation of the two envelope glycoprotein complexes even after a receptor-induced H-I98A reorganization has occurred. Either scenario is compatible with our observation that exposure of H-I98A F complexes to membrane-integral or soluble receptor does not lead to the initiation of biochemically appreciable F-trimer refolding.

Because H-F111A could complement H-I98A or H-ΔCD46 functionally on a heterodimer level in previous complementation studies (8), we furthermore conclude that the H-F111A reorganization is not structurally dominant. For the related Nipah virus G attachment protein, rearrangements have been proposed based on exposure of an mAb epitope after receptor docking (35) and altered mAb reactivity after stalk mutagenesis (34). Because crystals of free and receptor-complexed G head domains show few structural differences (36), changes in the G oligomer organization likewise may lead to Nipah F triggering, suggesting that basic principles of fusion initiation indeed may be conserved across different *Paramyxovirinae* genera.

Last, additional conditions located downstream of receptor binding and the initial F triggering must be fulfilled for productive MeV F refolding and fusion pore formation. Conceivably, these requirements could comprise a demand for a defined proximity of donor and target membrane provided by the continued interaction of H with membrane-embedded receptor, the coordinated local assembly of multiple activated H/F complexes through receptor clustering in the target membrane, a requirement for additional physical force originating from H/receptor-driven local curvature in opposing donor and target membranes (37, 38), or, potentially a second contact between attachment and refolding F protein complexes (39) that is required to complete membrane merger but is not induced through the interaction of H with soluble receptor.

In conclusion, we postulate that the functional MeV membrane fusion machinery is comprised of preassembled H-F heterooligomers in a prereceptor-bound/F-triggering H tetramer and prefusion F trimer conformation (Fig. 8*D*). Upon ligand binding to at least one of the covalent dimer pairs in the H dimer-of-dimers, partial unwinding/unraveling of the central section of the H stalk domain ensues, most likely disrupting preexisting contacts between the stalk and the F trimer. Little energy is required for this

step, because docking of soluble receptor moieties initiates the process efficiently. The resulting change in microenvironment at the former H–F contact zone may be sufficient for F refolding to commence. Unwinding of the stalk center most likely coincides with a rearrangement of the H head domain dimer–dimer interface. However, the overall physical integrity of the H tetramer and the tetrameric arrangement of the upper section of the H stalk remain intact during the process.

Methods

Cell Lines, Viral Stocks and Transfections. Vero (African green monkey kidney epithelial) cells (CCL-81; ATCC) and Vero cells stably expressing human SLAM [Vero-SLAM cells (40)] were maintained in DMEM supplemented with 7.5% (vol/vol) FBS at 37 °C and 5% CO_2. At every third passage, Vero-SLAM cells were kept under G418 selection. Lipofectamine 2000 (Invitrogen) was used for all transient transfection reactions. Modified vaccinia virus Ankara expressing T7 polymerase (41) was amplified in DF-1 (chicken embryo fibroblast) cells (CRL-12203; ATCC).

Site-Directed Mutagenesis and Epitope Tagging. Site-directed mutagenesis was performed following the QuikChange protocol (Stratagene) using pCG-H (42) as template. In addition, mutant constructs were epitope tagged, resulting in a set of H variants that contained either an N-terminal HA tag or a triple FLAG tag (43). A single or double copy of a single-chain antibody directed against the carcinoembryonic antigen (CEA) (25) was added to the H C terminus in some experiments to impart a significant change in molecular weight of the protein. Changes were confirmed by DNA sequencing in all cases.

Flow Cytometry for Analysis of H Expression and Receptor-Binding Capacity. Surface-expression levels of MeV H and the ability of MeV H variants to bind the SLAM receptor were monitored in a flow cytometer assay as previously described (6).

Quantitative Cell-to-Cell Fusion Assays. Cell-to-cell fusion was assessed using an established luciferase reporter assay as previously described (6, 8). For qualitative assessment, transfected Vero cells were photographed at the indicated times following transfection at a magnification of 200×. To quantify the extent of cell-to-cell fusion after partial reduction of engineered H disulfide bonds through DTT treatment, the number of nuclei present in discrete cells and in syncytia was quantified in multiple, randomly selected fields of view (magnification: 200×). The number of nuclei present in syncytia was determined by the difference in the number of individual cells counted in the negative control (F-only population) and the treated samples.

Statistical Analysis. To assess the statistical significance of differences between sample means, unpaired two-tailed *t* tests were applied using the Prism 5 (GraphPad) software package.

Envelope Glycoprotein Heterodimer Coimmunoprecipitation. Vero cells were transfected with equal amounts of the differently tagged H variants as indicated. Thirty-six hours posttransfection, cell-surface proteins were biotinylated with 0.5 mg/mL sulfosuccinimidyl-2-(biotinamido)ethyl-1,3-dithiopropionate (Thermo Scientific) for 20 min at 4 °C as previously described (6). Cleared supernatants were incubated with M2 mAb directed against the FLAG epitope (Sigma) at 4 °C. After precipitation with immobilized protein G at 4 °C, samples were washed and eluted in PBS, 2% SDS. The eluted material was diluted to 0.15% SDS with PBS, followed by adsorption of biotinylated protein material to immobilized streptavidin for 120 min at 4 °C. Bound material was eluted and denatured with urea buffer [200 mM Tris (pH 6.8), 8 M urea, 5% (wt/vol) SDS, 0.1 mM EDTA, 0.03% bromophenol blue, 1.5% (wt/vol) DTT] for 30 min at 50 °C, fractionated by SDS/PAGE, and blotted to PVD membranes. Immunoblots were decorated with α-FLAG (M2) and αHA (16b12) monoclonal antibodies, respectively, and were developed using an anti-mouse IgG light-chain conjugate and ChemiDoc XRS digital imaging system (Bio-Rad).

Detection of Envelope Glycoprotein Dimers on Cell Surface. Vero cells were transfected with 4 μg per well of MeV H-encoding DNA total, 2 μg of a FLAG-tagged H variant, and 2 μg of FLAG-tagged H variants containing a single-chain antibody moiety (XL) as indicated. Thirty-six hours posttransfection, cell-surface proteins were biotinylated with 0.5 mg/mL sulfosuccinimidyl-2-(biotinamido)ethyl-1,3-dithiopropionate as detailed above. Precipitates were washed as outlined above, split into two equal fractions, and denatured in urea buffer under reducing [urea buffer containing 1.5% (wt/vol) DTT] or nonreducing (urea buffer without DTT) conditions. Reduced samples were fractionated on 10% (wt/vol) SDS-Tris/glycine gels. Nonreduced samples were analyzed on 3–8% (wt/vol) NuPAGE Tris/Acetate gradient gels (Invitrogen).

Attachment Protein Homodimer Heterotetramer Gel-Shift Analysis. Vero cells were transfected with a total of 4 μg per well of MeV H-encoding DNA [1 μg encoding FLAG-tagged H variants and 3 μg encoding FLAG-tagged H featuring, in addition, a tandem copy of a single-chain α-CEA antibody (2XL)]. Thirty-six hours posttransfection, cells were subjected to native-PAGE analysis. Blots were visualized with α-FLAG M2 antibodies as described.

Cysteine Engineering and Assessment of Covalent H Tetramer Formation. Vero cells were transfected with 4 μg per well of MeV H-encoding plasmid DNA harboring individual cysteine substitutions as specified. Thirty-six hours posttransfection, cell-surface–exposed proteins were biotinylated as described. After precipitation with immobilized streptavidin, bound material was divided into two equal fractions, denatured under reducing (urea-DTT) or nonreducing (urea without DTT) conditions, and fractionated on 10% (wt/vol) SDS-Tris/glycine or 3–8% (wt/vol) NuPAGE Tris-Acetate gradient gels (Invitrogen). For densitometric analysis of immunoblots, signal intensities were quantified using the QuantityOne software package (Bio-Rad). The extent of covalent H tetramer formation was quantified by calculating for each individual mutant the ratio of H tetramer to total H material.

Native-PAGE and Native Gel Shift. Vero cells were transfected with 4 μg per well of plasmid DNA encoding different H constructs as specified. Thirty-six hours posttransfection, cells were washed with PBS, and protein was extracted using Native Tris Sample buffer [100 mM Tris·Cl, 10% glycerol, 0.0025% Bromophenol Blue (pH 8.6) with 0.1% digitonin] at 4 °C for 30 min. Samples were cleared (20,000 × *g* for 20 min) and fractionated on native-PAGE 3–12% (wt/vol) Bis-Tris gradient gels. PVDF blots were fixed with an 8% acetic acid wash for 10 min, followed by immunostaining and developing as outlined above.

For gel-shift experiments, antibodies (as specified) or affinity-purified soluble mouse Fc-SLAM receptor [sSLAM at 0.05 mg/mL final concentration (6)] were bound to H-protein–expressing cells on ice for 30 min before washing and digitonin extraction of proteins. In ex vivo binding experiments, digitonin extracts of H variants were prepared first and then were mixed with antibodies or sSLAM and incubated on ice for 30 min. In both cases, extracts were processed and subjected to native PAGE analysis as before.

Coimmunoprecipitation. To assess physical association of MeV H and F proteins, coimmunoprecipitation was carried out as previously described (6, 8).

In Situ Assessment of F Triggering. Vero cells were cotransfected with H-ΔCD46– and F-encoding plasmids, followed by incubation in the presence of fusion inhibitory peptide (FIP) as indicated to prevent any premature breakdown of the cell monolayer. Thirty-six hours posttransfection, cells were washed extensively to remove FIP and were subjected to surface immunoprecipitations by incubating intact monolayers in the presence of mAb [α-Flag M2 (Sigma) for control, α-pretrigger F(32), or α-triggered F(31); 1:750-dilution in DMEM each] at 4 °C to block conformational rearrangements of membrane-integral envelope glycoprotein complexes) or 37 °C to enable fusion for 1 h. Where specified, wells also received sSLAM or unspecific murine IgG (Sigma) at 0.05 mg/mL final concentration. Reference wells were overlaid with SLAM-positive Vero-SLAM cells before incubation at 37 °C. Subsequently, samples were incubated further for 1 h at 4 °C. Unbound antibody then was removed through extensive washing, cells were lysed in RIPA buffer, and cleared lysates were subjected to precipitation of immunocomplexes with immobilized protein G Sepharose and SDS/PAGE analysis as described above.

Dual Split-Protein Cell-Content–Mixing Assay. Vero cells were transfected with plasmids encoding H-ΔCD46, F, and dual-split protein (DSP_{1-7}) (33). In controls, H-encoding plasmid was omitted. A second population of Vero or Vero-SLAM cells was transfected with plasmids encoding SLAM and DSP_{8-11} (33) or DSP_{8-11} alone. As a reference for reconstitution of N-terminal (DSP_{1-7}) and C-terminal (DSP_{8-11}) GFP/renilla luciferase halves, controls were cotransfected with both DSP_{1-7} and DSP_{8-11} plasmids. Twenty-four hours posttransfection, cells were mixed at an equal ratio in the specified combinations and reseeded in black-walled 96-well plates; specified wells received sSLAM at 0.05 mg/mL final concentration. Cell-content mixing indicating fusion pore formation was monitored over a 12-h time window at 37 °C by following DSP_{1-7} and DSP_{8-11} reconstitution resulting in restored renilla luciferase activity. As substrate, EnduRen (Promega) was added according to the manufacturer's

instruction. Plates were examined at 90-min intervals in a BioTek Synergy H1 plate reader in luminescence top-count area scan mode. For each replicate, relative luciferase units were calculated through normalization of individual measurements for the maximum readout found in the DSP_{1-7}/DSP_{8-11} double-transfected reference cell population. In some experiments, cell populations were reseeded into 12-well plates and incubated in the presence or absence of additional sSLAM (0.05 mg/mL final concentration), and fusion was assessed microscopically.

ACKNOWLEDGMENTS. We thank B. Horvat and M. Ehnlund for providing mAbs directed against the MeV F protein and G. Melikyan, N. Kondo, and Z. Matsuda for providing split-luciferase reporter plasmids. This work was supported, in part, by National Research Service Award/National Institute of Allergy and Infectious Disease (NIAID) F32 AI085763 from the National Institutes of Health (NIH)/NIAID (to M.A.B.) and by Public Health Service Grant AI083402 from the NIH/NIAID (to R.K.P.).

1. Lamb RA, Jardetzky TS (2007) Structural basis of viral invasion: Lessons from paramyxovirus F. *Curr Opin Struct Biol* 17:427–436.
2. Deng R, Mirza AM, Mahon PJ, Iorio RM (1997) Functional chimeric HN glycoproteins derived from Newcastle disease virus and human parainfluenza virus-3. *Arch Virol Suppl* 13:115–130.
3. Deng R, Wang Z, Mirza AM, Iorio RM (1995) Localization of a domain on the paramyxovirus attachment protein required for the promotion of cellular fusion by its homologous fusion protein spike. *Virology* 209:457–469.
4. Melanson VR, Iorio RM (2006) Addition of N-glycans in the stalk of the Newcastle disease virus HN protein blocks its interaction with the F protein and prevents fusion. *J Virol* 80:623–633.
5. Tanabayashi K, Compans RW (1996) Functional interaction of paramyxovirus glycoproteins: Identification of a domain in Sendai virus HN which promotes cell fusion. *J Virol* 70:6112–6118.
6. Paal T, et al. (2009) Probing the spatial organization of measles virus fusion complexes. *J Virol* 83:10480–10493.
7. Lee JK, et al. (2008) Functional interaction between paramyxovirus fusion and attachment proteins. *J Biol Chem* 283:16561–16572.
8. Brindley MA, Plemper RK (2010) Blue native PAGE and biomolecular complementation reveal a tetrameric or higher-order oligomer organization of the physiological measles virus attachment protein H. *J Virol* 84:12174–12184.
9. Hashiguchi T, et al. (2011) Structure of the measles virus hemagglutinin bound to its cellular receptor SLAM. *Nat Struct Mol Biol* 18:135–141.
10. Colf LA, Juo ZS, Garcia KC (2007) Structure of the measles virus hemagglutinin. *Nat Struct Mol Biol* 14:1227–1228.
11. Santiago C, Celma ML, Stehle T, Casasnovas JM (2010) Structure of the measles virus hemagglutinin bound to the CD46 receptor. *Nat Struct Mol Biol* 17:124–129.
12. Hashiguchi T, et al. (2007) Crystal structure of measles virus hemagglutinin provides insight into effective vaccines. *Proc Natl Acad Sci USA* 104:19535–19540.
13. Noyce RS, et al. (2011) Tumor cell marker PVRL4 (nectin 4) is an epithelial cell receptor for measles virus. *PLoS Pathog* 7:e1002240.
14. Hashiguchi T, Maenaka K, Yanagi Y (2011) Measles virus hemagglutinin: Structural insights into cell entry and measles vaccine. *Front Microbiol* 2:247.
15. Plemper RK, Hammond AL, Cattaneo R (2001) Measles virus envelope glycoproteins hetero-oligomerize in the endoplasmic reticulum. *J Biol Chem* 276:44239–44246.
16. Corey EA, Iorio RM (2007) Mutations in the stalk of the measles virus hemagglutinin protein decrease fusion but do not interfere with virus-specific interaction with the homologous fusion protein. *J Virol* 81:9900–9910.
17. Plemper RK, Brindley MA, Iorio RM (2011) Structural and mechanistic studies of measles virus illuminate paramyxovirus entry. *PLoS Pathog* 7:e1002058.
18. Yuan P, et al. (2011) Structure of the Newcastle disease virus hemagglutinin-neuraminidase (HN) ectodomain reveals a four-helix bundle stalk. *Proc Natl Acad Sci USA* 108:14920–14925.
19. Bose S, et al. (2011) Structure and mutagenesis of the parainfluenza virus 5 hemagglutinin-neuraminidase stalk domain reveals a four-helix bundle and the role of the stalk in fusion promotion. *J Virol* 85:12855–12866.
20. Yuan P, et al. (2005) Structural studies of the parainfluenza virus 5 hemagglutinin-neuraminidase tetramer in complex with its receptor, sialyllactose. *Structure* 13: 803–815.
21. Plemper RK, Hammond AL, Cattaneo R (2000) Characterization of a region of the measles virus hemagglutinin sufficient for its dimerization. *J Virol* 74:6485–6493.
22. Feige MJ, Hendershot LM (2011) Disulfide bonds in ER protein folding and homeostasis. *Curr Opin Cell Biol* 23:167–175.
23. Patterson JB, Scheiflinger F, Manchester M, Yilma T, Oldstone MB (1999) Structural and functional studies of the measles virus hemagglutinin: Identification of a novel site required for CD46 interaction. *Virology* 256:142–151.
24. Corey EA, Iorio RM (2009) Measles virus attachment proteins with impaired ability to bind CD46 interact more efficiently with the homologous fusion protein. *Virology* 383:1–5.
25. Hammond AL, et al. (2001) Single-chain antibody displayed on a recombinant measles virus confers entry through the tumor-associated carcinoembryonic antigen. *J Virol* 75:2087–2096.
26. Reisinger V, Eichacker LA (2008) Solubilization of membrane protein complexes for blue native PAGE. *J Proteomics* 71:277–283.
27. Corbin JD, et al. (2011) Metal ion stimulators of PDE5 cause similar conformational changes in the enzyme as does cGMP or sildenafil. *Cell Signal* 23:778–784.
28. Zettler J, Mootz HD (2010) Biochemical evidence for conformational changes in the cross-talk between adenylation and peptidyl-carrier protein domains of nonribosomal peptide synthetases. *FEBS J* 277:1159–1171.
29. Connolly SA, Leser GP, Yin HS, Jardetzky TS, Lamb RA (2006) Refolding of a paramyxovirus F protein from prefusion to postfusion conformations observed by liposome binding and electron microscopy. *Proc Natl Acad Sci USA* 103:17903–17908.
30. Ader N, et al. (2012) Structural rearrangements of the central region of the morbillivirus attachment protein stalk domain trigger F protein refolding for membrane fusion. *J Biol Chem* 287:16324–16334.
31. Malvoisin E, Wild F (1990) Contribution of measles virus fusion protein in protective immunity: Anti-F monoclonal antibodies neutralize virus infectivity and protect mice against challenge. *J Virol* 64:5160–5162.
32. Sheshberadaran H, Chen SN, Norrby E (1983) Monoclonal antibodies against five structural components of measles virus. I. Characterization of antigenic determinants on nine strains of measles virus. *Virology* 128:341–353.
33. Kondo N, Miyauchi K, Matsuda Z (2011) Monitoring viral-mediated membrane fusion using fluorescent reporter methods. *Curr Protoc Cell Biol*, Chapter 26:26.9.1–26.9.9.
34. Bishop KA, et al. (2008) Residues in the stalk domain of the hendra virus g glycoprotein modulate conformational changes associated with receptor binding. *J Virol* 82:11398–11409.
35. Aguilar HC, et al. (2009) A novel receptor-induced activation site in the Nipah virus attachment glycoprotein (G) involved in triggering the fusion glycoprotein (F). *J Biol Chem* 284:1628–1635.
36. Xu K, et al. (2008) Host cell recognition by the henipaviruses: Crystal structures of the Nipah G attachment glycoprotein and its complex with ephrin-B3. *Proc Natl Acad Sci USA* 105:9953–9958.
37. Plemper RK (2011) Cell entry of enveloped viruses. *Curr Opin Virol* 1:92–100.
38. Melikyan GB (2011) Membrane fusion mediated by human immunodeficiency virus envelope glycoprotein. *Curr Top Membr* 68:81–106.
39. Porotto M, et al. (2011) Spring-loaded model revisited: Paramyxovirus fusion requires engagement of a receptor binding protein beyond initial triggering of the fusion protein. *J Virol* 85:12867–12880.
40. Ono N, et al. (2001) Measles viruses on throat swabs from measles patients use signaling lymphocytic activation molecule (CDw150) but not CD46 as a cellular receptor. *J Virol* 75:4399–4401.
41. Sutter G, Ohlmann M, Erfle V (1995) Non-replicating vaccinia vector efficiently expresses bacteriophage T7 RNA polymerase. *FEBS Lett* 371:9–12.
42. Cathomen T, Naim HY, Cattaneo R (1998) Measles viruses with altered envelope protein cytoplasmic tails gain cell fusion competence. *J Virol* 72:1224–1234.
43. Zhang L, Hernan R, Brizzard B (2001) Multiple tandem epitope tagging for enhanced detection of protein expressed in mammalian cells. *Mol Biotechnol* 19:313–321.

JVI
Journals.ASM.org

HIV-1 Infection *Ex Vivo* Accelerates Measles Virus Infection by Upregulating Signaling Lymphocytic Activation Molecule (SLAM) in $CD4^+$ T Cells

Yu-ya Mitsuki,[a] Kazutaka Terahara,[a] Kentaro Shibusawa,[a] Takuya Yamamoto,[b] Takatsugu Tsuchiya,[a] Fuminori Mizukoshi,[a] Masayuki Ishige,[a,c] Seiji Okada,[c] Kazuo Kobayashi,[a] Yuko Morikawa,[d] Tetsuo Nakayama,[e] Makoto Takeda,[f] Yusuke Yanagi,[g] and Yasuko Tsunetsugu-Yokota[a]

Department of Immunology, National Institute of Infectious Diseases, Shinjuku-ku, Tokyo, Japan[a]; Immunology Laboratory, Vaccine Research Center, National Institute of Allergy and Infectious Diseases, National Institutes of Health, Bethesda, Maryland, USA[b]; Center for AIDS Research, Kumamoto University, Kumamoto, Japan[c]; Laboratory of Viral Infection II, Kitasato Institute for Life Science, Kitasato University, Tokyo, Japan[d]; Laboratory of Viral Infection I, Kitasato Institute for Life Science, Kitasato University, Tokyo, Japan[e]; Department of Virology III, National Institute of Infectious Diseases, Tokyo, Japan[f]; and Department of Virology, Faculty of Medicine, Kyushu University, Fukuoka, Japan[g]

Measles virus (MV) infection in children harboring human immunodeficiency virus type 1 (HIV-1) is often fatal, even in the presence of neutralizing antibodies; however, the underlying mechanisms are unclear. Therefore, the aim of the present study was to examine the interaction between HIV-1 and wild-type MV (MVwt) or an MV vaccine strain (MVvac) during dual infection. The results showed that the frequencies of MVwt- and MVvac-infected $CD4^+$ T cells within the resting peripheral blood mononuclear cells (PBMCs) were increased 3- to 4-fold after HIV-1 infection, and this was associated with a marked upregulation of signaling lymphocytic activation molecule (SLAM) expression on $CD4^+$ T cells but not on $CD8^+$ T cells. SLAM upregulation was induced by infection with a replication-competent HIV-1 isolate comprising both the X4 and R5 types and to a lesser extent by a pseudotyped HIV-1 infection. Notably, SLAM upregulation was observed in HIV-infected as well as -uninfected $CD4^+$ T cells and was abrogated by the removal of HLA-DR^+ cells from the PBMC culture. Furthermore, SLAM upregulation did not occur in uninfected PBMCs cultured together with HIV-infected PBMCs in compartments separated by a permeable membrane, indicating that no soluble factors were involved. Rather, $CD4^+$ T cell activation mediated through direct contact with dendritic cells via leukocyte function-associated molecule 1 (LFA-1)/intercellular adhesion molecule 1 (ICAM-1) and LFA-3/CD2 was critical. Thus, HIV-1 infection induces a high level of SLAM expression on $CD4^+$ T cells, which may enhance their susceptibility to MV and exacerbate measles in coinfected individuals.

The attenuated measles virus (MV) vaccine has greatly reduced the morbidity and mortality of measles in industrialized countries. However, measles is still a leading cause of death among children in developing countries, especially in sub-Saharan Africa, where almost 90% of global pediatric human immunodeficiency virus type 1 (HIV-1) infections occur (http://apps.who.int/ghodata/). Because both HIV-1 and MV cause immunosuppression, it is conceivable that coinfection with HIV-1 and MV increases the risk of disease progression (17). In fact, an observational study of hospitalized children in Zambia showed that the fatality rate increased among HIV-1-infected children with measles (18).

The low levels of neutralizing antibodies in HIV-1-infected children may explain the high mortality of measles. The measles vaccine is only weakly immunogenic in HIV-1-infected children, inducing only low levels of neutralizing antibody, which decline rapidly (17). However, a recent large-scale prospective study in Zambia conducted by Moss et al. reported a good initial antibody response to measles vaccine in both HIV-1-infected and -uninfected children (19). Moreover, to understand the impact of HIV-1 infection on the clinical manifestation of measles, Permar et al. conducted a study using MV-vaccinated or -unvaccinated rhesus monkeys that are chronically infected with a simian immunodeficiency virus (24). They monitored the virological and immunological status of the monkeys after MV challenge and found that the clinical manifestation of measles occurs even in monkeys with high titers of vaccine-induced MV neutralizing antibody. This finding implies that the presence of neutralizing antibody alone is not sufficient protection from measles in HIV-1-infected individuals. Therefore, it is highly likely that an as yet unknown factor(s)/mechanism(s) affected by HIV-1 is involved in the exacerbation of measles in HIV-1-infected individuals.

Some studies analyzed the interaction between MV and HIV-1 *in vitro*. Garcia et al. studied HIV-1 replication in peripheral blood mononuclear cells (PBMCs) coinfected with MV and found that MV-induced inhibition of lymphocyte proliferation suppresses HIV-1 replication, but without any apparent increase in the production of chemokines or any other soluble factors in coinfected cultures (7). In a more recent study, the same group demonstrated that the cell cycle progression of T cells, which is required for efficient HIV-1 replication, was blocked by MV (8); however, it is still not clear whether HIV-1 affects MV infection directly or indirectly.

Understanding the impact of HIV-1 infection on MV infection

Received 28 October 2011 **Accepted** 10 April 2012
Published ahead of print 24 April 2012
Address correspondence to Yasuko Tsunetsugu-Yokota, yyokota@nih.go.jp.
Supplemental material for this article may be found at http://jvi.asm.org/.

doi:10.1128/JVI.06681-11

and replication is important both for developing successful strategies for measles eradication and for HIV-1 control. The receptor for wild-type MV has been identified to be signaling lymphocytic activation molecule (SLAM; also known as CD150), and attenuated vaccine strains can utilize both SLAM and CD46 (4). Recently, nectin4 was also identified as an MV receptor that is important for MV to spread into epithelial cells and release viral particles from the apical membrane into the lumen of the respiratory tract (20, 21). However, SLAM remains a major receptor of MV in lymphoid organs and plays an important role in a systemic MV infection. Therefore, the aim of the present study was to investigate the course of MV infection in HIV-1-infected PBMCs *ex vivo* at the level of the individual cell, focusing on SLAM expression. The results presented here showed that HIV-1 replication in resting PBMCs induces the upregulation of SLAM expression on $CD4^+$ T cells in a manner that is dependent on cell-to-cell contact, resulting in higher levels of MV infection.

MATERIALS AND METHODS

Cell preparation. Human peripheral blood samples were collected from healthy donors after receiving written informed consent. Sample collection was approved by the institutional ethical committee of the National Institute of Infectious Diseases (Tokyo, Japan). PBMCs were separated by Ficoll-Hypaque density gradient centrifugation (Lymphosepal; IBL, Gunma, Japan). T cells were isolated using a total T cell enrichment kit (StemCell Technologies, Vancouver, BC, Canada), after depletion of $CD14^+$ cells. For monocyte depletion, $CD14^+$ cells were depleted from PBMCs using magnetically activated cell sorting (MACS) with CD14 microbeads (Miltenyi Biotec, Cologne, Germany). For B cell and HLA-DR^+ cell depletion, PBMCs were incubated with biotin-labeled anti-CD19 (BioLegend, San Diego, CA) and biotin-labeled anti-HLA-DR (BioLegend) antibodies, respectively, followed by positive selection using anti-biotin tetrameric antibody complex (TAC), magnetic colloid, and an EasySep magnet (all from StemCell Technologies).

Preparation of virus stock. To prepare HIV-1 clones HIV-$1_{NL\text{-}E}$, HIV-$1_{NLAD8\text{-}E}$, and HIV-$1_{NL\text{-}D}$, human 293T embryonic kidney cells seeded at a density of 7×10^6 cells/15-cm dish were transfected with 30 μg of pNL-E, pNLAD8-E, and pNL-D, respectively, using the calcium phosphate precipitation method as described previously (29). To prepare HIV-1 pseudotyped with vesicular stomatitis virus glycoprotein (HIV-1/VSV-G), 293T cells were cotransfected with 36 μg of pNL-EdENV (pNL-E with an *env*-inactivating mutation) and 4 μg of pVSV-G per 7×10^6 cells. At 2 days posttransfection, the culture supernatant was collected, filtrated, and frozen at −80°C. The amounts of viruses in each culture supernatant were measured using an in-house HIV-1 Gag p24 enzyme-linked immunosorbent assay.

To prepare green fluorescent protein (GFP)-expressing wild-type (IC323-EGFP) (12) or vaccine strain (GFP-MVAIK) (6) MV, 1×10^7 human SLAM-expressing Vero cells (Vero/hSLAM) cells were infected with 1×10^5 PFU of each virus (multiplicity of infection [MOI] = 0.01) for 2 h, washed, and then grown in Dulbecco's modified Eagle medium (DMEM; Gibco, Carlsbad, CA) supplemented with 2% heat-inactivated fetal bovine serum (FBS). Infected cells were harvested when approximately 80% cytotoxicity was observed. Cells were then frozen and thawed three times and sonicated for 10 s to release the cell-bound viruses. The titer of measles virus was measured using a plaque assay, described in the following section.

Titration of MV. MV was titrated as described previously (26). In brief, monolayers of 2×10^5 Vero/hSLAM cells grown in 12-well plates were infected with serially diluted wild-type MV (MVwt) or an attenuated MV vaccine strain (MVvac). After removal of viruses, the cells were overlaid with DMEM supplemented with 2% methylcellulose and 2% FBS. At day 5 postinfection, cells were stained with 5% neutral red, the numbers of plaques were counted, and the numbers of PFU/ml were calculated.

HIV-1 and MV infection. For HIV-1 infection, untreated PBMCs or PBMCs depleted of either $CD14^+$ monocytes, $CD19^+$ B cells, or HLA-DR^+ cells or purified T cells (1×10^6 cells) were infected with 100 ng of p24 of either HIV-$1_{NL\text{-}E}$, HIV-$1_{NL\text{-}D}$, HIV-$1_{NLAD8\text{-}E}$, or HIV-1/VSV-G for 2 h, washed three times with RPMI 1640 (RPMI), and then cultured in RPMI supplemented with 5% heat-inactivated human serum (P-RPMI), penicillin (100 μg/ml), and streptomycin (100 μg/ml). At day 3 postinfection, the culture medium was changed to 5% P-RPMI supplemented with interleukin-2 (IL-2; 50 U/ml) and then cultured for 2 days.

For MV infection, HIV-$1_{NL\text{-}D}$-infected and -uninfected PBMCs (1×10^6 cells) were mock infected or infected with 5×10^4 PFU of either MVwt or MVvac for 2 h at day 5 after HIV infection, washed three times with RPMI, and then cultured in 5% P-RPMI for 2 days.

Flow cytometry. Cells were stained with a suitable combination of fluorescence-labeled monoclonal antibodies (MAbs): Pacific Blue-labeled anti-CD4 (eBioscience, San Diego, CA), allophycocyanin (APC)-Cy7-labeled anti-CD8 (eBioscience), peridinin chlorophyll protein-labeled anti-CD3 (R&D Systems, Inc., Minneapolis, MN), APC-labeled anti-CD14 (R&D Systems), phycoerythrin (PE)-labeled anti-SLAM (eBioscience), and PE-Cy7-labeled anti-CD19 (BioLegend). Dead cells were visualized using a LIVE/DEAD fixable dead cell stain kit (Invitrogen, Carlsbad, CA). HIV-1- and/or MV-infected cells were analyzed using flow cytometry (FACSCant II flow cytometer; BD Bioscience, Pharmingen, CA) and a FACSDiva flow cytometer (BD Bioscience) or Flowjo software (Tree Star, San Carlos, CA).

Detection of cytokines. The levels of gamma interferon (IFN-γ), IL-1β, IL-2, IL-5, IL-10, tumor necrosis factor alpha (TNF-α), and TNF-β in the culture supernatant of the HIV-1-infected or mock-infected PBMC cultures were measured using a FlowCytomix human Th1/Th2 11plex kit (Bender MedSystems, Vienna, Austria), according to the manufacturer's protocol, at day 5 postinfection. The minimum detection levels for each cytokine were as follows: IFN-γ, 1.6 pg/ml; IL-1β, 4.2 pg/ml; IL-2, 16.4 pg/ml; IL-4, 20.8 pg/ml; IL-5, 1.6 pg/ml; IL-6, 1.2 pg/ml; IL-8, 0.5 pg/ml; IL-10, 1.9 pg/ml; IL-12 p70, 1.5 pg/ml; TNF-α, 3.2 pg/ml; and TNF-β, 2.4 pg/ml. Results were calculated using FlowCytomix Pro software (Bender MedSystems).

Transwell assay. HIV-1-infected or -uninfected PBMCs were cultured in the top chamber of a transwell plate (pore size, 0.4 μm; Costar; Corning, Corning, NY). HIV-1-uninfected PBMCs were placed on the bottom chamber and cultured for 5 days.

Blocking of antibodies against cell adhesion molecules. An isotype control IgG1 (PeproTech Inc., Rocky Hill, NJ) or serial dilutions of anti-leukocyte function-associated molecule 1α (anti-LFA-1α) or anti-LFA-3 MAbs (serially diluted from 10 μg/ml) were added to HIV-1-infected PBMC cultures just after 2 h of infection to analyze the effect of cell-to-cell contact on SLAM upregulation. Anti-LFA-1α and anti-LFA-3 MAbs were prepared from hybridomas kindly provided by Hideo Yagita (Juntendo University, Tokyo, Japan).

Statistical analysis. Because of the limited sample size, each experiment was performed once per donor. Data obtained from less than three donors were excluded from the statistical analysis. The significance of the data was evaluated by the Mann-Whitney U test, by the Tukey multiple-comparison test, or by use of the Pearson correlation coefficient on the basis of the normality and variance of the data using GraphPad Prism software (version 4.0; GraphPad Software, San Diego, CA). *P* values of <0.05 were considered statistically significant.

RESULTS

HIV-1 infection enhances the infectivity of coinfected MV *ex vivo*. First, the consequences of coinfection of PBMCs with HIV-1 and MV were analyzed at the single-cell level using flow cytometry. DsRed-expressing ($DsRed^+$) HIV-$1_{NL\text{-}D}$- or mock-infected PBMCs were coinfected with GFP-expressing (GFP^+) MVwt or

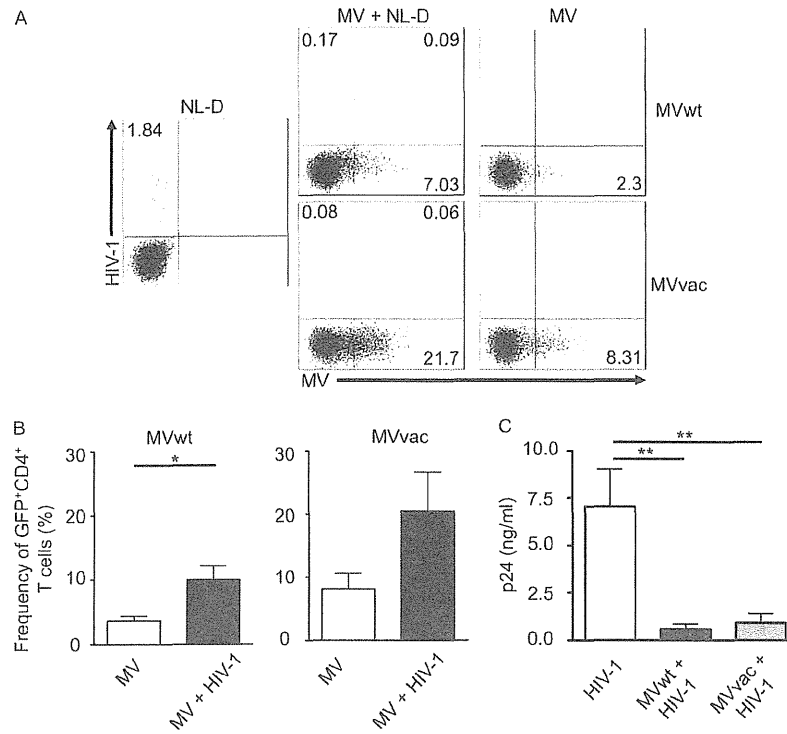

FIG 1 Effect of HIV-1 infection on MV infection in an *ex vivo* HIV-1/MV coinfection model. PBMCs were coinfected with HIV-1_{NL-D} and/or either MVwt or MVvac, and the infected cells were analyzed. (A) Representative flow cytometry plots showing MVwt- or MVvac-infected $CD4^+$ T cells. (B) Cumulative data showing the frequency of MVwt- or MVvac-infected $CD4^+$ T cells. The bars represent the mean ± SEM ($n = 7$). *P* values were calculated using the Mann-Whitney U test. *, $P < 0.05$. (C) Levels of p24 antigen in culture supernatants of HIV-1 and/or MV-infected PBMCs. The bars represent the mean ± SEM ($n = 5$). *P* values were calculated using one-way analysis of variance followed by the Tukey multiple-comparison test. **, $P < 0.01$.

MVvac at day 5. Two days later, HIV- and/or MV-infected cells were analyzed. As shown in Fig. 1A, HIV-1_{NL-D}-infected and MV-infected cells were identified as $DsRed^+$ and GFP^+ cells, respectively. In the case of MVwt infection, the frequency of MVwt-infected $CD4^+$ T cells within the HIV-1_{NL-D}-infected PBMC population (9.96% ± 2.45%) was significantly higher than that in the MV-only-infected PBMC population (3.60% ± 0.77%) ($P = 0.0175$; $n = 7$; Fig. 1B, left). Likewise, in the case of MVvac infection, the frequency of MVvac-infected $CD4^+$ T cells tended to be higher within the HIV-1_{NL-D}-infected PBMC population (20.42% ± 6.20%) than within the MV-only-infected PBMC population (8.14% ± 2.45%), although the result was not statistically significant ($P = 0.1158$; $n = 7$; Fig. 1B, right). These results indicated that HIV-1 infection enhances MV infection in PBMCs. It should be noted that the HIV-infected $CD4^+$ T cell population disappeared upon MV infection (from 1.84% to 0.26% and 0.14% for MVwt and MVvac, respectively), and the doubly infected $CD4^+$ T cell population was rarely visible (Fig. 1A). Although we used the same MOI, the percentage of MV-infected T cells was always higher in MVvac infection than in MVwt infection. This is probably due to the wider tropism of MVvac, which utilizes both SLAM and CD46 as receptors (4).

The level of HIV-1 Gag p24 in the culture supernatant was also significantly reduced by coinfection with either MVwt or MVvac compared with that observed after infection with HIV-1_{NL-D} alone ($P < 0.01$; $n = 5$; Fig. 1C). These results are consistent with those reported previously; i.e., MV infection inhibits the replication of HIV-1 (7, 8, 10).

SLAM expression on $CD4^+$ T cells is induced by HIV-1 infection. Because both MVwt and MVvac utilize SLAM as a receptor (5, 22), SLAM expression was examined in HIV-1-infected PBMCs. PBMCs were infected with either CXCR4-tropic HIV-1_{NL-E}, CCR5-tropic HIV-$1_{NLAD8-E}$, or HIV-1/VSV-G, all of which express GFP, and were then cultured for 5 days without additional stimulation (apart from the addition of IL-2). It is noteworthy that, regardless of HIV-1 infection, SLAM expression was slightly increased under these culture conditions at day 5 (basal increase), and this basal increase varied among individuals (5.17 ± 2.63% at day 0 to 8.81% ± 2.00% at day 5; $n = 7$). Therefore, the net increase in the frequency of $SLAM^{hi}$ $CD4^+$ or $SLAM^{hi}$ $CD8^+$ T cells was calculated by subtracting their respective basal levels of increase. Induction of SLAM expression on $CD8^+$ T cells was low and did not increase statistically significantly with HIV-1 infection (Fig. 2A, bottom, and B, right). However, importantly, both the level of SLAM expression and the frequency of $SLAM^{hi}$ $CD4^+$ T cells increased after infection with HIV-1, and increased SLAM expression was observed in HIV-1-infected (GFP^+) as well as in uninfected $CD4^+$ T cells (Fig. 2A, top). Because the net increase in SLAM expression varied between donors, PBMCs from 10 donors were examined. The frequency of $SLAM^{hi}$ $CD4^+$ T cells markedly increased in the HIV-1_{NL-E}-infected cultures (8.79% ± 1.47%), while the frequency in HIV-1/VSV-G-infected cultures increased only slightly (2.52% ± 0.58%). This difference between HIV-1_{NL-E}- and HIV-1/VSV-G-infected cultures was statistically significant ($P < 0.01$; $n = 10$; Fig. 2B). Of note, HIV-1/VSV-G-infected